

**DESIGN RECOMMENDATIONS FOR HSS-TO-WTEE CONNECTIONS
IN LONG-SPAN TRI-CHORD STRUCTURES**

by

Ying Li

B.E. in Civil Engineering, Wuhan Urban Construction Institute, 1997

M.E. in Structural Engineering, Tongji University, 2001

**Submitted to the Graduate Faculty of
School of Engineering in partial fulfillment
of the requirements for the degree of
Master of Science of Civil Engineering**

University of Pittsburgh

2003

UNIVERSITY OF PITTSBURGH

SCHOOL OF ENGINEERING

This thesis was presented

by

Ying Li

It was defended on

March 14, 2003

and approved by

Dr. Jeen-Shang Lin, Associate Professor, Department of
Civil and Environmental Engineering

Dr. John F. Oyler, Adjunct Associate Professor, Department of
Civil and Environmental Engineering

Thesis Advisor: Dr. Christopher J. Earls, Associate Professor, Department of
Civil and Environmental Engineering

ABSTRACT

DESIGN RECOMMENDATIONS FOR HSS-TO-WTEE CONNECTIONS IN LONG-SPAN TRI-CHORD STRUCTURES

Ying Li, MS

University of Pittsburgh, 2003

Tri-chord sign structures are a frequently used sign type within the Commonwealth of Pennsylvania. However, due to the recent failure of this sign type during erection in PENNDOT district 6, the HSS-to-TEE connection response near the tri-chord structure tower has become a focus of concern.

The present research first surveys existing literature related to the types of failure modes that govern in the connection regions of hollow circular Hollow Structural Sections (HSS). Then finite element modeling strategies are identified and subsequently verified using the experimental testing report of Thomas J. Boone et al. (1982). These validated modeling techniques are then employed to simulate the response of the considered HSS-to-WTEE connection region. Bearing capacities and failure modes are obtained for representative design cases commonly used in the Commonwealth.

Based on the simulation results, a simplified, design office-type equation for predicting the WTEE bearing capacity of circular HSS members is formulated utilizing several

approximations in conjunction with the yield-line theory. In addition, the nominal HSS-to-TEE connection capacities from the AISC Manual of Steel Construction (Third Edition) and AISC Hollow Structural Sections Connection Manual (AISC 1997) are evaluated for accuracy. It is found that nominal capacity in a circular HSS members loaded by a uniformly distributed line loading of finite length may successfully be applied for the prediction of connection capacity in HSS-WTEE joints that are consistent with those scenarios considered in current research.

FOREWORD

This thesis is the culmination of a deal of effort and support by many individuals.

First of all, I would like to express my gratitude to my research advisor, Dr. Christopher J. Earls, for his support, patience and guidance. Next, I must thank my committee members, Dr. Jeen-Shang Lin and Dr. John F. Oyler, for serving on my committee and for being kind.

I also want to thank all my friends and fellow students for their constant support and encouragement along the way. I will always remember the good times spent with them.

This thesis is dedicated to my family. I thank my father Li GuoSheng, my mother Wu XiaoJuan, my older sister Li Ping and brother-in-law Zhu GuangYu for their help throughout the years.

TABLE OF CONTENTS

ABSTRACT.....	iii
FOREWORD.....	v
LIST OF TABLES.....	ix
LIST OF FIGURES.....	x
1.0 INTRODUCTION.....	1
1.1 Origin of Problem.....	1
1.2 Statement of Problem.....	6
1.3 Scope of Study.....	9
2.0 LITERATURE REVIEW.....	10
2.1 Earlier Behavioral Research.....	10
2.1.1 “Buckling Strength of Circular Tubes” by Schilling.....	10
2.1.2 HSS Strength Predication Research by Davies and Packer.....	18
2.1.3 Joint Connection Researchs.....	19
2.2 Existing Design Standards.....	23
2.3 Test Report Suitable for FEM Validation.....	25
3.0 NONLINEAR FINITE ELEMENT ANALYSIS.....	26
3.1 Sources of Nonlinearity	26
3.2 Nonlinear Analysis.....	26

3.3 True Stress and Logarithmic Strain.....	28
4.0 VERIFICATION STUDY	30
4.1 Verification Test	30
4.1.1 Specimens and Test Setup.....	30
4.1.2 Instrumentation	33
4.1.3 Tests.....	35
4.2 ABAQUS Modeling.....	37
4.3 Study of Results from Experiments & ABAQUS.....	41
4.3.1 Results Comparison.....	41
4.3.2 Discussion of Comparison Results.....	51
4.4 Conclusion	52
5.0 WTEE BEARING MODEL.....	53
5.1 Statement of Problem.....	53
5.2 WTEE Bearing Model.....	54
5.3 Results from WTEE Bearing Model.....	58
6.0 WTEE BEARING CAPACITY ESTIMATION.....	61
6.1 Estimation of WTEE Bearing Capacity.....	61
6.1.1 Assumptions and Approximations.....	61
6.1.2 Deducing the Estimation Equation	62
6.1.3 Bearing Capacity from the Estimation Equation.....	67
6.1.3.1 Case-1.....	67
6.1.3.2 Case-2.....	68
6.2 Connection Capacity from AISC.....	69

6.2.1 HSS-to-TEE Connection Capacity.....	69
6.2.2 Longitudinally Bearing Capacity from AISC.....	76
6.3 Discussion of Results.....	77
7.0 CONCLUSIONS AND RECOMMENDATIONS.....	79
7.1 Validity of ABAQUS Modeling Techniques.....	79
7.2 Yield-Line based Capacity Estimation Equation.....	79
7.3 Checking WTEE Bearing Capacity Using the AISC Specification.....	80
7.4 Flat Bearing Seat Connection Problem.....	81
APPENDICES.....	82
APPENDIX A.....	83
APPENDIX B.....	90
BIBLIOGRAPHY.....	92

LIST OF TABLES

Table 4.1 Comparison of Result from Tests and ABAQUS.....	41
Table 6.1 Connection Cases Considered.....	70
Table 6.2 TEE Properties.....	70
Table 6.3 TEE Flexural Buckling Capacity.....	71
Table 6.4 TEE Flexural-Torsional Buckling Capacity.....	72
Table 6.5 HSS Shear Capacity.....	73
Table 6.6 HSS Bearing Capacity.....	74
Table 6.7 HSS-to-TEE Connection Capacity.....	75
Table 6.8 Comparison of Predicted WTEE Bearing Connection Capacities.....	77

LIST OF FIGURES

Figure 1.1 2-Column Tri-Chord Sign Structure Elevation.....	3
Figure 1.2 4-Cloumn Tri-Chord Sign Structure Elevation.....	4
Figure 1.3 4-Column Tri-Chord Sign Tower Elevation.....	5
Figure 1.4 Configuration of Saddle Seats	7
Figure 1.5 Close-up Photograph of District 12 Tri-Chord Connection Retrofit.....	7
Figure 1.6 Photograph of District 12 Tri-Chord Connection Retrofit.....	8
Figure 4.1 Specimen Geometry Details.....	31
Figure 4.2 Location of Dial Gages and Inclinometers.....	34
Figure 4.3 Elevation View of Experimental Branch Specimen A1 & AP5.....	36
Figure 4.4 Constitutive Law Used in Finite Element Verification Studies.....	40
Figure 4.5 Comparison of ABAQUS and experimental results: Test A1.....	43
Figure 4.6 Comparison of ABAQUS and experimental results: Teat AP5.....	43
Figure 4.7 Deformed Geometry of Specimen A1 from Experimental Testing.....	44
Figure 4.8 Deformed Geometry of Specimen A1 from ABAQUS.....	45
Figure 4.9 Deformed Geometry of Specimen AP5 from Experimental Testing.....	46
Figure 4.10 Deformed Geometry of Specimen AP5 from ABAQUS.....	47
Figure 4.11 Comparison of Models with Perfect and Imperfect Geometry.....	49
Figure 4.12 Comparison of ABAQUS Models With MPC and Without MPC.....	49

Figure 5.1 Overall Geometry and Loading of WTEE Bearing Model	55
Figure 5.2 Constitutive Law Used in WTEE Bearing Model.....	57
Figure 5.3 Representative Yield-Line Formation in WTEE Bearing Model -1.....	59
Figure 5.4 Representative Yield-Line Formation in WTEE Bearing Model -2.....	60
Figure 6.1 Bearing Capacity Estimation Model.....	62
Figure 6.2 Yield Lines of HSS Mechanism.....	63
Figure 6.3 Detailed Initial & Failure Geometries of HSS Mechanism.....	63
Figure 6.4 Simplified Mechanism Model.....	64
Figure 6.5 M_p Calculation Plot.....	65
Figure 6.6 Schematic of HSS in Case -1.....	67
Figure 6.7 Schematic of HSS in Case -2.....	68

1.0 INTRODUCTION

1.1 Origin of Problem

For the proper functioning of the surface transportation system, signage is required to alert the motoring public to changes in: interstate topology, weather conditions, traffic patterns, as well as for other informational purposes. Along heavily traveled segments of the interstate system in urban areas, the roadway is particularly wide so as to accommodate the required number of travel lanes needed to address heavy regional traffic volumes. In such situations, highway signs must span great distances (e.g. from 18,000 *mm* (or 59.06 *ft*) to 72,000 *mm* (or 236.22 *ft*)) in pursuit of a safe means for providing the motorist with needed information without introducing the danger associated with the occurrence of intermediate supports on medians, or other locations adjacent to the roadway. In such instances, a design scenario frequently employed within the Commonwealth of Pennsylvania is the tri-chord sign structure.

As seen in Figure 1.1 and Figure 1.2, the tri-chord sign structure consists of two sets of columns that serve as supports for elevated bridging upon which signage is attached. There are frequently either one or two HSS columns per side in the overall sign structure geometry. Typically, the four-column configuration is used in longer span versions for the tri-chord sign structure type, and the two-column one in shorter span versions. The bridging typically is a latticework, triangular in cross-section, where three circular Hollow Structural Sections (HSS) occur at the three vertices of the triangle with angle and/or WTEE structural sections composing the lacings that attach the three HSS members to one another.

The connections of the lacing members to the circular HSS members are typically achieved through the use of gusset plates proportioned such that the lines of action of all forces, or the neutral axes of lacing members, introduced into a given connection region intersect at the

same point on the center line of the circular HSS; thus supporting an analytical approximation that the bridging is a space truss with pinned joints. As a result of this truss-like construction within the bridging, the three circular HSS members assume the role of truss chord members and hence the name “tri-chord” sign is justified.

The connection region where the tri-chord truss is attached to the columns experiences very large forces as a result of dead loads from sign panels and light fixtures, etc., as well as the action of environmental forces from wind or ice, etc. The general attachment between the columns and tri-chord truss occurs through the ends of the tri-chord HSS members, bearing directly on seats and U-bolts (as shown in Figure 1.3 for a four-column configuration), or bearing on curved saddle blocks (that will be described later). It is the performance of this connection region that is at issue within the scope of this thesis.

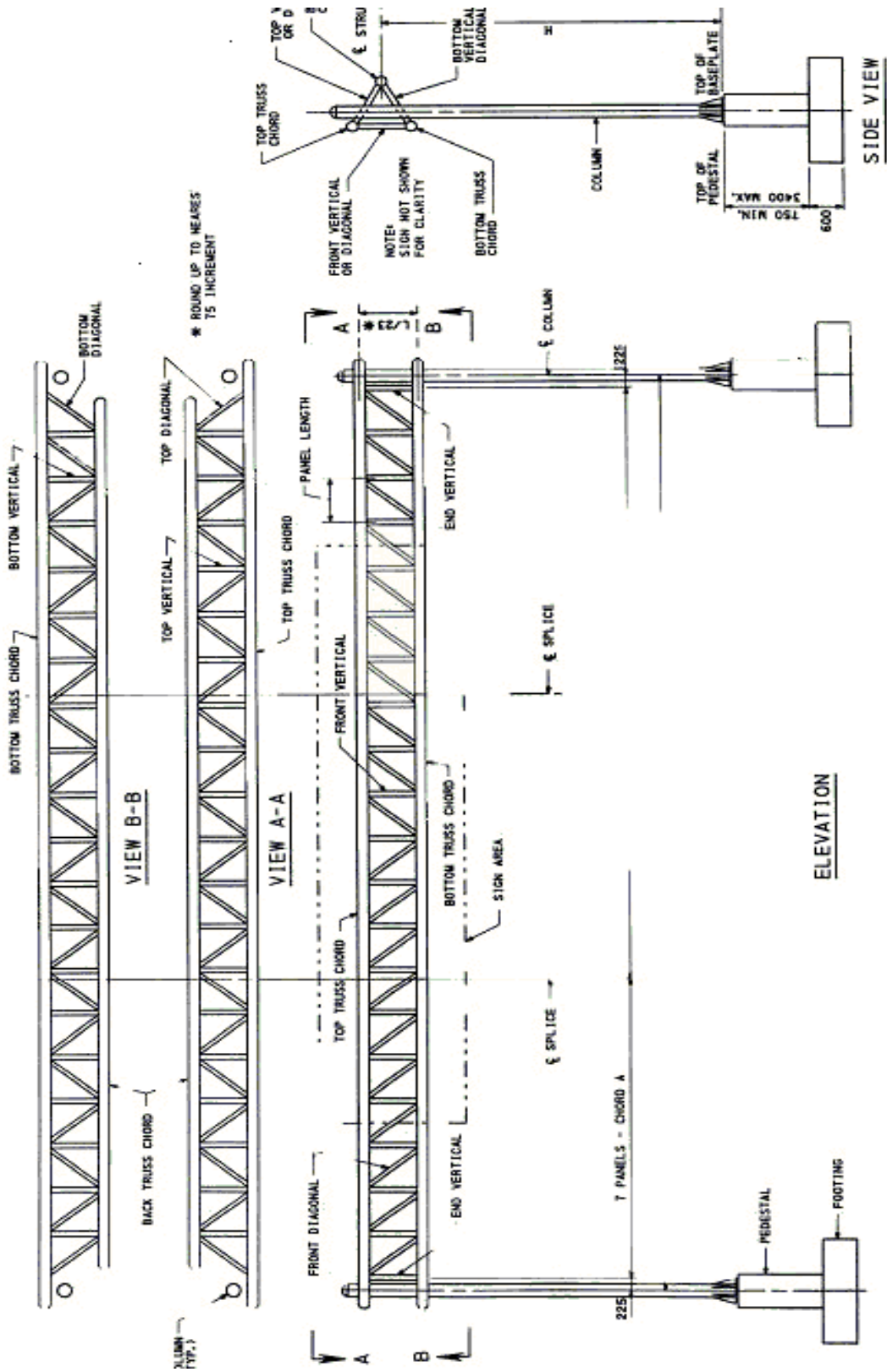


Figure 1.1 2-Column Tri-Chord Sign Structure Elevation

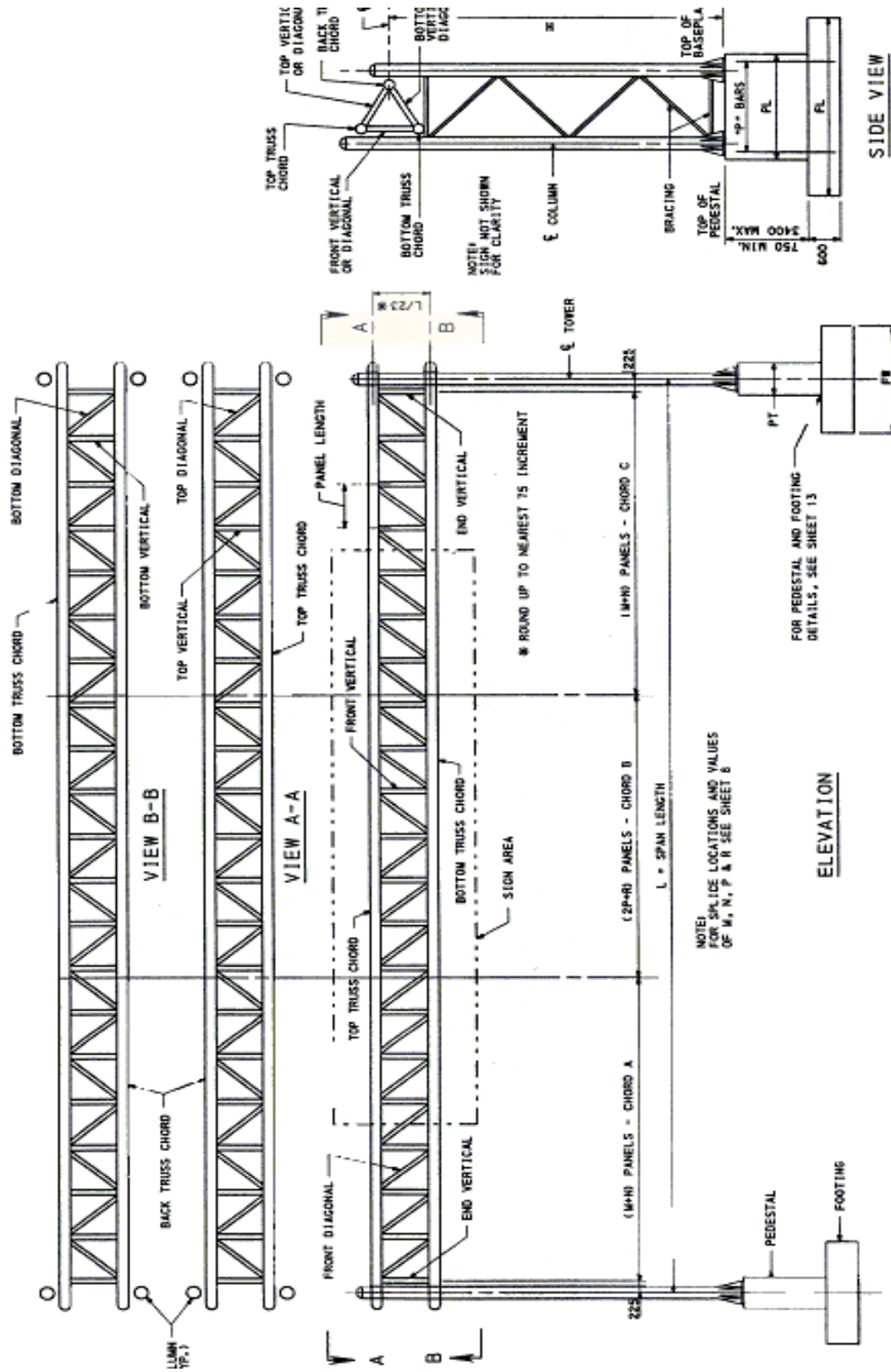


Figure 1.2 4-Column Tri-Chord Sign Structure Elevation

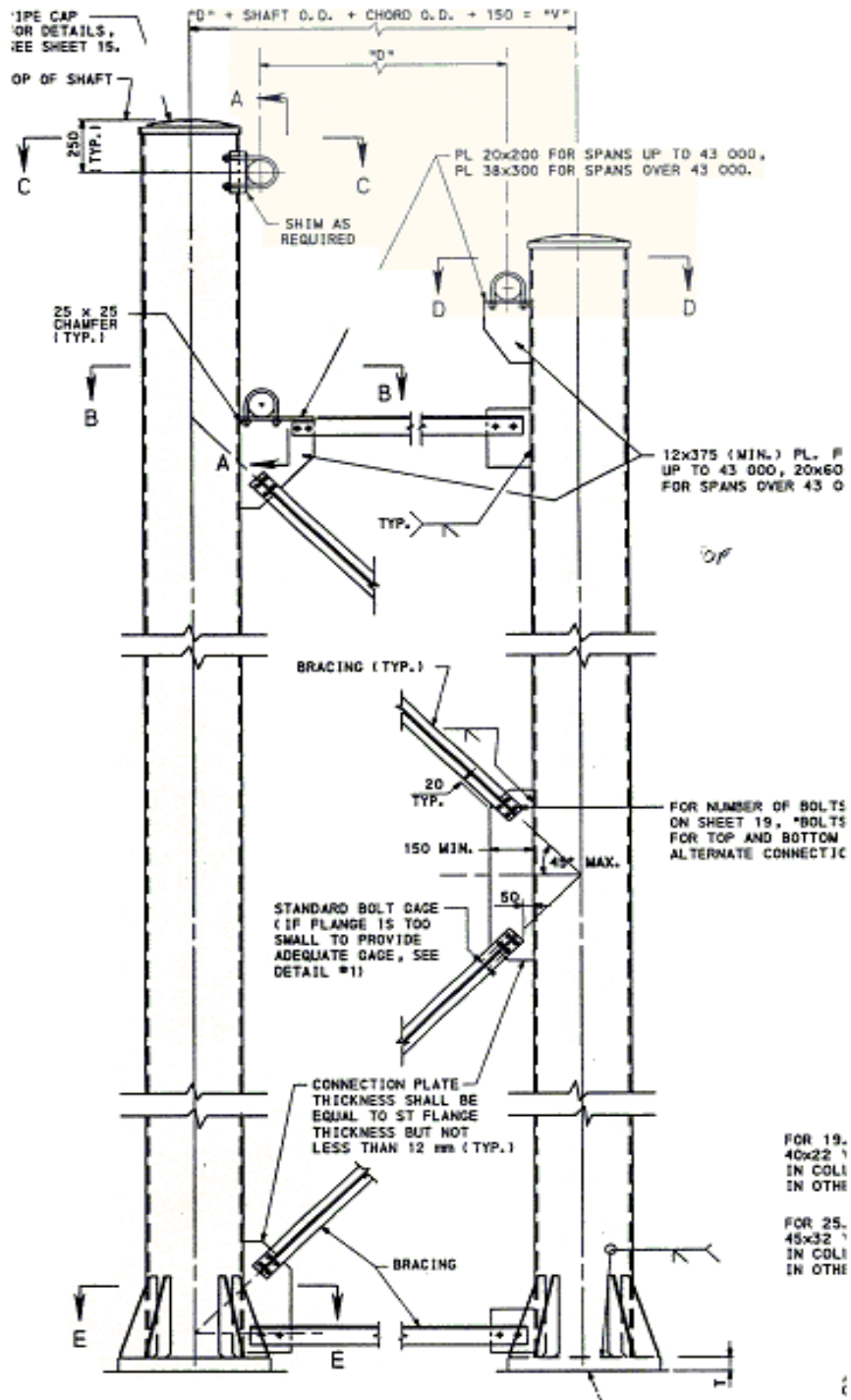


Figure 1.3 4-Column Tri-Chord Sign Tower Elevation

1.2 Statement of Problem

The Bridge Quality Assurance Division of the Pennsylvania Department of Transportation's (PENNDOT's) Bureau of Design has expressed concern that the current tri-chord sign structure design standards in place (BD-644M, PENNDOT 1996 and the AASHTO Specification 2001) are not safe and economical when applied to long-span tri-chord sign structures. This sentiment comes on the heels of a recent failure in PENNDOT District 6 where a tri-chord sign structure with a 180 *ft* (or 54,864 *mm*) span experienced a crushing failure at the HSS chord-column connections during final erection. A similar sign structure with a 140 *ft* (or 42,672 *mm*) span was scheduled to be erected in District 12 shortly thereafter. As a result of the failure in District 6, the District 12 job was delayed while modifications were made to the connection region details.

The resulting District 6 design retrofit consisted of cutting out the damaged section of HSS in each lower chord connection side and installing a new piece with a 100 percent greater wall thickness than the original piece, in addition to containing a series of two annular plate stiffeners at each column seat location. A further corrective measure within the District 6 retrofit was to employ curved saddles upon which the circular HSS bear (see Figure 1.4). Hence, the overall contact area of the chord at the column attachment increases beyond what was originally specified. In the case of the District 12 sign structure, the circular HSS chord ends were filled with non shrink grout and seated on a series of fabricated saddles instead of bearing directly on the flat surface of a standard seat connection (see Figure 1.5 and Figure 1.6).

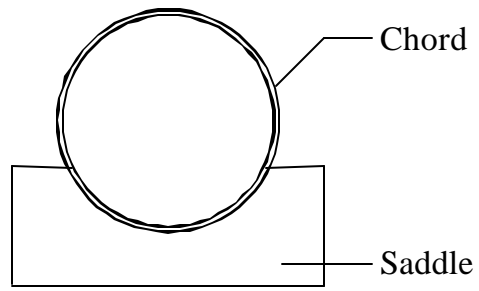


Figure 1.4 Configuration of Saddle Seats



Figure 1.5 Close-up Photograph of District 12 Tri-Chord Connection Retrofit



Figure 1.6 Photograph of District 12 Tri-Chord Connection Retrofit

While the retrofits in District 6 and 12 are believed to be adequate for preventing any additional problems with crushing of the portion of the circular HSS wall bearing on the column seat, a more rigorous understanding of the mechanics in the connection region is sought in order that more economical and reliable design provisions can be prescribed, both within the context of the American Association of State Highway and Transportation Officials specification (AASHTO 2001) and BD-644M (PENNDOT 1996). Furthermore, now that the circular HSS crushing failure model has to some extent been mitigated at the location of the seat, as a result of the retrofits discussed before, the focus of concern now shifts to the reserve capacity within the lattice uprights of the chord lacing immediately adjacent to the connection region.

1.3 Scope of Study

The first part of the current thesis is focused on surveying the existing literature related to the types of failure modes that govern in the connection regions of tri-chord sign structures. Beyond the literature review, an investigation of the failure that occurred in District 6, within the context of current AISC LRFD provisions related to the failure mode observed, is carried out. As a result of the preceding study of the problem under investigation, finite element modeling strategies are identified and subsequently verified using relevant experimental research results from the literature. These validated modeling techniques are then employed in a study of the connection region utilizing yield-line theory. The aim is providing insight for the identification of a simplified manual strength calculation strategy for easy design office use. Recommendations related to design practice are subsequently made.

Hence, the effort research is focused on: formulating and validating a useful nonlinear finite element modeling technique; using the validated finite element modeling techniques to

simulate the response of the considered HSS-to-WTEE connection region; using the simulation results to formulate a simplified, design office-type equation for predicting the WTEE bearing capacity of circular HSS.

2.0 LITERATURE REVIEW

The present literature review is organized along three distinct lines of focus related to the current research investigation aimed at evaluating the adequacy of existing design practice applied to the connection regions of tri-chord highway sign structures. The respective focus areas are: 1) earlier research dealing directly with the behavioral issues associated with limit states of import in tri-chord sign structures; 2) existing specification provisions related to specific limit states that arise within the region in question; 3) earlier experimental studies lending themselves to usage in a verification study wherein the validity of the nonlinear finite element modeling strategies employed in the current research may be assessed.

2.1 Earlier Behavioral Research

2.1.1 “Buckling Strength of Circular Tubes” by Schilling

The paper “Buckling Strength of Circular Tubes” by Schilling (1965) was motivated by the then lack of special treatment of circular tubes in the buckling provisions of design specifications. The purpose of the paper was to summarize the available information on the buckling of circular tubes; compare various design methodologies from different disciplines; and for cases in which these design methodologies differ widely, test results were used to determine correctness.

Schilling begins the paper with a brief discussion related to the two types of stress-strain response that are typical of steel used in tube construction: yield point and “round-house.” The yield point type of steel material response is the classical behavior covered in elementary textbooks wherein the steel has a well-defined yield point that is immediately followed by a distinct yield plateau that precedes strain-hardening behavior. However, in the case of “round-

house” response, a gradual transition from elastic to inelastic material response characterizes the mechanical response. In this latter type of material response, the gradual transition from elastic to inelastic response means that no definite yield point is observable. In addition, no yield plateau is observed to occur.

Following the discussion of material response, Schilling describes the three dominant methodologies whereby steel tubes are manufactured: seamless tube construction; welded construction; and cold-expanded or cold-worked.

In seamless tube construction, the steel mechanical response is of the yield point type. However, the presence of residual stresses from uneven cooling may cause gross cross-sectional yielding response at a stress levels at or above 75 percent of the material yielding stress.

Welded types are formed by either cold or hot forming of plate into a tube section and then subsequently employing a longitudinal weld down the seam to close the section. In the case of cold forming and welding, the material response will most likely be of a “round-house” type with a proportional limit for the cross-section being 50 percent of the yield point for the particular grade used in the plate from which the tube is fabricated. For the hot forming, followed by butt-welding of the plate ends to close the section, the steel mechanical response is more closely aligned with the yield point response and Schilling indicates that this case may be treated in the same way as the seamless tube.

The case of cold-expanded or cold-worked tubes involves a hot rolled tube that is expanded in the circumferential direction when cold. This type of tube construction results in a “round-house” mechanical response as a result of the combined effects of cold working, Bauschinger effect, and residual stresses.

After the discussion of common fabrication and manufacturing techniques, Schilling goes on to treat commonly encountered limit states arising in structural steel tube design applications: column buckling and local buckling. In each case Schilling approaches the design problem using a single factor of safety, which was consistent with the working stress design philosophy that dominated at that time.

For the case of column buckling, Schilling introduces the standard Euler buckling equation with several approximations that simplify the calculation of the governing radius of gyration. This classical Euler buckling approach is then extended for use in the inelastic range through the notion of tangent modulus. The significant effects of residual stresses on overall column buckling response can be accounted for through the execution of stub-column tests on short lengths tubular cross-section, from which an aggregate axial stress-strain response, for the entire cross-section, may be obtained and employed in the tangent modulus component of the Euler equation as follows in Equation 2-1 below:

$$f'_{cr} = \frac{\mathbf{P}^2 E_T}{(0.2kL/R)^2} \quad (2-1)$$

where E_T is the tangent modulus obtained from the stub-column tests, and R is the radius of the tube. The influence of the inevitable geometric imperfection associated with column out-of-straightness is accounted for within the factor of safety of the design equations.

In the case of the contemporary AISC and AASHTO specifications at the time when the paper was published, the column buckling approach of the Column Research Council (CRC) was adopted. The CRC approach recognized the fact that the stub-column response of any given cross-section would have a profound impact on the nature of the inelastic transition region associated with intermediate column slenderness ratios. As a result of this understanding, the

CRC equation for hot-rolled I-shaped columns was based on theoretical calculations associated with stub-column behavior and the resulting equations took the form of Equation 2-2:

$$f_a = \frac{f_y}{N} \left[1 - \frac{f_y}{4\mathbf{p}^2 E} \left(\frac{kL}{r} \right)^2 \right] \quad (2-2)$$

Where N is the factor of safety that varies from 1.67 to 1.92 as a function of column slenderness C_c . The equation for N appears as Equation 2-3 and the column slenderness C_c as Equation 2-4.

$$N = \frac{5}{3} + \frac{3(kL/r)}{8C_c} - \frac{(kL/r)}{8C_c^3} \quad (2-3)$$

$$C_c = \sqrt{\frac{2\mathbf{p}^2 E}{f_y}} \quad (2-4)$$

Schilling discusses the specialization of the above design equations for use with electric resistance welded steel tubes possessing yield strengths of between 45 and 55 *ksi* and with elastic proportional limit of approximately 50 percent of yield. In such a case, Equation 2-2 and Equation 2-4 can be specialized to be of the form of Equation 2-5 and Equation 2-6 below per as Wolford and Rebholz (1958).

$$f_a = \frac{f_y}{N} \left[1 - 0.385 \frac{f_y}{\mathbf{p}^2 E} \left(\frac{kL}{r} \right)^2 \right] \quad (2-5)$$

$$C_c = 1.73 \sqrt{\frac{\mathbf{p}^2 E}{f_y}} \quad (2-6)$$

Under the rubric of local buckling, Schilling discusses instances involving pure compression, bending, torsion, transverse shear, and combined loading. Schilling's discussion in places closely parallels the work of Gerard (1962). This parallel begins with the adoption of Gerard's classification of circular tubes into three categories according to slenderness: short tubes; moderate tubes; and long tubes. A curvature limit-type relation is at the heart of the classification system and is presented as Equation 2-7.

$$Z = \left(\frac{R}{t} \right) \left(\frac{L}{R} \right)^2 (1 - u^2)^{1/2} \quad (2-7)$$

If the typical value for Poisson's ratio u is substituted as 0.3, then Equation 2-7 is simplified to be:

$$Z = 0.954 \left(\frac{R}{t} \right) \left(\frac{L}{R} \right)^2 \quad (2-8)$$

Schilling notes that for the case of short tubes, the local buckling strength tends to be related to both the R/t and L/R ratios. In contrast, moderate tubes display a local buckling behavior that depends primarily upon R/t (a notable exception to this is the case of torsion induced local buckling wherein the local buckling response again depends on both L/R and R/t with the former ratio having the greatest influence in this case). The long tube category buckling manifestation is closely related to the overall compressive response treated during the development of Equation 2-5 and Equation 2-6 above.

In the remainder of Schilling's local buckling treatment he takes a conservative approach by considering only moderate tubes. Schilling points out that consideration of moderate tubes is most appropriate "because: 1) tubes used in such applications usually are in the moderate-length

region, and 2) the local buckling strength of a tube of a given R/t is a minimum if the tube is in the moderate-length region.”

For the case of local buckling in compression within moderate tubes (i.e. those with a $Z > 2.85$) the critical compressive stress is given by:

$$f_{cr} = aCE \frac{t}{R} \quad (2-9)$$

where

$$C = \frac{1}{\sqrt{3(1-u^2)}} \quad (2-10)$$

and

$$a = \left(\frac{1-u^2}{1-u_p^2} \right)^{1/2} \left(\frac{E_s}{E} \right) \left(\frac{E_t}{E} \right)^{1/2} \quad (2-11)$$

where, E_s is the secant modulus which varies in relation to the amount that f_{cr} exceeds the proportional limit for the column. Furthermore, u_p is the Poisson's ratio in the plastic range (for typical incompressible solids this value is 1/2). Making the assumption of plastic range incompressibility in conjunction with the assumption that the elastic range Poisson's ratio is 0.3 leads to a simplification of Equation 2-11:

$$a = 1.10 \frac{\sqrt{E_s E_t}}{E} \quad (2-12)$$

Schilling points out in the paper that the foregoing local buckling predictive equations for the pure compression case may be conservatively extended to the flexural buckling case. An amplification factor of 1.3 should be applied to the critical stress for the pure compression case to account for the more favorable stress distribution in a cross-section under flexure.

In his treatment of torsion induced local buckling, Schilling once again considers tubes of moderate length to be most appropriate for general conservative provisions and as such treats tubes with Z values between 50 and $9(R/t)^2$. The theoretical local buckling strength for moderate tubes loaded in torsion is then presented as:

$$V_{cr} = \frac{0.596a}{(1-u^2)^{5/8}} E \left(\frac{t}{R} \right)^{5/4} \left(\frac{R}{L} \right)^{1/2} = 0.632aE \left(\frac{t}{R} \right)^{5/4} \left(\frac{R}{L} \right)^{1/2} \quad (2-13)$$

in which V_{cr} is the shear stress causing buckling and a is the plasticity reduction factor given by

$$a = \left(\frac{1-u^2}{1-u_p^2} \right)^{3/4} \left(\frac{E_s}{E} \right) = 1.16 \frac{E_s}{E} \quad (2-14)$$

It is important to point out that in the development of Equation 2-13, a 15 percent reduction factor is applied to account for the effects of initial imperfections on the experimentally observed critical load for tubes in torsion as compared with theoretical predictions. Since Equation 2-13 is also predicated in the presence of simple boundary conditions, when applying this equation to tubes with built-in ends a 10 percent amplification factor should be applied to account for the favorable post-buckling response exhibited by this case.

When considering pure shear loading in the development of local buckling in circular tubes, Schilling notes that the experimental data related to this case tends to be, on average, 60 percent higher than for the case of pure torsion in the same tube. Presumably the stress gradient condition in the pure shear case is less severe than the stress state present in the tube subjected to pure torsion. However, a 25 percent increase may be applied as an extremely conservative

amplification factor since this value represents the lowest observed capacity from any test, whereas the previous 60 percent value was average over all tests.

2.1.2 HSS Strength Predication Research by Davies and Packer

A study focusing on strength prediction, within branch plate rectangular hollow steel sections, is outlined in the paper by Davies and Packer (1982). While the focus of the paper is on rectangular hollow sections, and not circular hollow cross-sections as is the focus of the present research, the paper is important nonetheless for its analytical approach.

The analytical approach employed by Davies and Packer is an extension of the classical yield line approach used in conjunction with the Upper Bound Plastic Limit Theorem, which may be stated as: “A [collapse] load computed on the basis of an assumed mechanism will always be greater than, or equal to, the true plastic limit load” (ASCE 1971). Examples of the classical yield line approach to ultimate strength prediction in rectangular hollow structural steel sections are contained in the work of Kapp (1974), Packer et al. (1980, 1982), and Stockwell (1974, 1975). The approach summarized by Davies and Packer is a departure from the former studies in that punching shear is considered in conjunction with the formation of the yield-line based collapse mechanism. The punching shear effect is considered through the inclusion of shear energy terms within the overall energy balance equations used to identify the collapse load. As with the classical yield line approach, the approach employed by Davies and Packer develops the kinematics of the collapse mechanism from the problem geometry under consideration in addition to consideration of the effects that the punching shear has on the trajectories of the yield lines that impinge on the zones of punching shear.

The study compares experimental results with predictions made using the modified yield line approach. What was observed in these comparisons is that the punching shear modifications considered enhances the ability of yield line theory to predict actual measured responses in experiments. A further conclusion is that the notion of so-called “efficiency” in a tubular connection (the ratio of the width of the connecting plate to the width of the tube wall) is essentially a meaningless quantity that can be ignored for the purposes of design.

2.1.3 Joint Connection Researchs

The paper by Frater and Packer (1992) focuses on resolving discrepancies that exist between the predicted deflections in hollow structural section trusses obtained using standard linear elastic analysis techniques assuming pin jointed connections and deflections obtained from laboratory testing; typically lab testing results in deflections that are between 12 percent to 15 percent greater than theoretical predictions (Czechowski et al. 1984, Philiastides 1988, Coutie and Saidani 1989, 1991). What Frater and Packer (1992) have undertaken in the research project outlined in their paper is a program of carefully designed and executed full-scale testing of 12.0 *m* and 12.2 *m* spans, simply supported Warren Trusses comprised of 60 degree gap, or overlap, K-connections. What they have ultimately learned in this research is that for the purposes of design, a linear, elastic pinned jointed analysis of the truss is adequate for the determination of internal member forces in the truss. However, if deflections are to be accurately modeled then joint kinematics and flexibility must be considered in the analysis. Frater and Packer have developed a reasonably accurate means for doing this based on the principle of virtual work.

The approach used by Packer and Frater is not entirely new however. Czechowski et al. (1984) devised a technique wherein a micro-bar model, consisting of three rigid bars forming a

mechanism that is stabilized by springs, is used within a standard matrix structural analysis context for the purposes of simulated chord face deflections. The micro-bar linkage of Czechowski et al. (1984) considers three degrees of freedom: translational; translational-rotational; and rotational. As a result of the joint restraint arising from the only three admissible chord deflection modes, the joint model of Czechowski et al. (1984) properly captures the secondary moments that frequently arise in actual gap jointed K-connection geometries in hollow structural section trusses and hence the agreement between the model and full-scale experiments is excellent.

In contrast to this finding though, Philiastides (1988) compares three analytical models (differing only in the manner in which the joints are modeled) and full-scale experimental results. In the analytical modeling, the three cases considered are: full joint rigidity; full joint moment release; and a micro-bar model using some flexible bar members to provide realistic joint stiffness (in contrast to the rigid bar – spring models of Czechowski et al. (1984)). What Philiastides observes is paraphrased by Frater and Packer (1992): 1) “Axial force distributions were similar using all three methods, but underestimated the experimental distributions slightly”; 2) the micro-bar and rigid joint models gave reasonable estimations of the elastic chord bending moments, but both methods poorly predicted web member moments (the micro-model predicting better than the rigid joint model); 3) “truss deflections by both the pin-jointed and rigid joint models were similar in magnitude to one another, but less than the experimental value. The micro-bar model represented a more flexible theoretical structure, but even this model underestimated truss deflection by 15 percent.” Philiastides (1988) also concluded that the micro-bar model in hollow structural truss analysis does not necessarily generate more accurate axial force-bending moment-truss deflection patterns than a simple pinned-jointed analysis. This

is in contrast to the findings of Czechowski et al. (1984) in which a distinct improvement is noted with the use of the micro-bar model.

Coutie and Saidani (1989, 1991) utilize a sophisticated finite element approach to the proper theoretical modeling of joints in hollow structural section joints. In their finite element models, Coutie and Saidani (1989, 1991) model chord and web members with two-nodded beam elements, and the connection region with eight-nodded plate elements. In later models, weldments have also been modeled using solid elements. In this latter case, semiloof shell elements have been substituted for the plate elements within the connection regions so as to maintain mesh compatibility at the element transition interfaces. As a result of this modeling, Coutie and Saidani (1989, 1991) are able to conclude: “1) Pin-jointed analysis is satisfactory for theoretical predictions of axial force; 2) Rigid-jointed analysis is satisfactory for theoretical predictions of chord moments in a 100 percent overlap-connected truss, while in a gap-connected truss it can be misleading. In the case of web moments, a rigid-jointed analysis gives poor results for both gap- and overlap-connected trusses. A semi rigid analysis, including modeling of the weld, gives a much better prediction of the chord and web member moments; 3) For a gap-connected truss, a semi-rigid analysis overestimates the central deflection by three percent, while a rigid-jointed analysis underestimates it by 19 percent. Frater and Packer (1992)”

Lau (1987) takes a different approach to the modeling of the chord face deformations in that the principle of virtual work is employed to arrive at a suitable flexibility coefficient that may be used in the matrix structural analysis of a hollow structural section truss. This approach is adopted by Frater and Packer (1992) and subsequently extended to include the overt consideration of connection eccentricity through the inclusion of a rigid link element pinned at

the end attached to the web members and rigidly connected to the chord member, which for the purposes of this modeling is considered to be continuous over the entire span of the truss.

Based on careful full-scale experimentation and analytical modeling incorporating ideal pinned, ideal fixed, and flexibility coefficient derived joint response, the following conclusions are made by Frater and Packer (1992): “1) A simple pin-jointed analysis is sufficient to give good predictions for the web and chord member axial forces; 2) The theoretical distribution of bending moments based on a rigid model and a pinned-rigid model showed a poor numerical agreement with the experimental moments in the chords. However, in design, it might only be necessary to predict the maximum chord moment and check its interaction with the maximum axial force. For this purpose the pinned-rigid model was generally successful. Also, the magnitudes of the member moments generated in the trusses tested were low relative to the member axial forces, as only panel point loading was used. Hence under these load conditions the accurate prediction of bending moments is not essential. However, for trusses loaded between panel points, significant bending moments will be produced in the compression cord, and in such cases the pinned-rigid model is recommended; 3) The theoretical truss deflections have been shown to be similar in magnitude for all three models used in the analysis, but underestimate real truss deflections by nine percent-20 percent. However, it has been shown that one can achieve an excellent estimate for the theoretical truss deflections by adding truss deflection due to connection flexibility to that for the pinned jointed truss analysis. Before this technique can be used extensively in design, it will be necessary to establish sufficient HSS connection deformation data for the development of parametric formulae giving the flexibility associated with various connections. The connection flexibility data reported in this paper represent a contribution to this endeavor.”

2.2 Existing Design Standards

The AISC Hollow Structural Sections Connections Manual (1997) is the definitive American design manual representing the state-of-the-art in hollow structural section connection design and detailing. This manual treats specific design topics related to: dimensions and properties of HSS members; welding practice; issues related to bolting; simple shear connections; moment connections; tension and compression connections; cap plates, base plate, and column splices; and welded truss connections. In addition, the manual contains the AISC Specification for the Design of Hollow Structural Sections (1997), which is a design standard dealing specifically with the design issues related to: material properties; loads and load combinations; effective net area for tension members; local plate buckling; limiting slenderness ratios; and design for tension, compression, flexure, shear, torsion, combined loading, and the localized effects of various type of transverse loading scenarios; weld design; truss connection design; and fabrication requirements.

The AISC Hollow Structural Sections Connections Manual (1997) has a Canadian counterpart in the CISC Hollow Structural Section Connections and Trusses Design Guide (1997). This Canadian Manual treats many of the same topics of its American counterpart as well as several additional topics such as: material property and cross-sectional geometric definitions; standard truss design; standard truss welded connections; non-standard truss design; multiplanar welded connections; HSS to HSS moment connections; bolted HSS connections; fabrication, welding, and inspection; beam to HSS column connections; trusses and base plates to HSS connections; plate to HSS connections; HSS welded connections subjected to fatigue loading; and standard truss examples.

While it may appear from the forgoing that the Canadian and American HSS manuals are very similar, this would be an incorrect conclusion to draw. The American HSS manual (AISC 1997) is constructed to be very much consistent with the format and fundamental approach contained in all other AISC design manuals and as such takes a much more general approach to the promulgation of design guidelines. In contrast, the Canadian HSS manual (Packer and Henderson 1997) is much more focused on the specific design case of the HSS truss. Most of the Canadian manual is focused to support the design of variations on the HSS truss form.

The provisions within the AISC Hollow Structural Sections Manual (1997), as contained in subsection 8.2 *Concentrated Force Distributed Longitudinally at the Center of the HSS Face*, are most germane to the present discussion. The nominal capacity of a circular HSS subjected to a longitudinally distributed uniformly line load is:

$$R_n = 5F_y t^2 \left(1 + \frac{N}{4D} \right) Q_f \quad (2-15)$$

where,

F_y = minimum specified yield stress of the HSS

t = design HSS wall thickness

D = outside diameter of round HSS

N = bearing length of the load along the length of the HSS

Q_f = 1.0 for tension in the HSS

= $1 - 0.3 f/F_y - 0.3 (f/F_y)^2 \leq 1.0$ for compression in the HSS

This equation is in turn a direct copy of the “Factored Connection Resistances” presented in table 11.2 within the Canadian HSS manual (Packer and Henderson 1997).

2.3 Test Report Suitable for FEM Validation

As part of the conduct of the present research, a means of validating the modeling methodology employed is sought. To this end, the experimental testing report of Thomas J. Boone et al. (1982) is an ideal candidate for consideration within the context of an analytical verification study since the researchers were careful to report many significant, yet subtle, details of their experimentation thus allowing for the appropriate modeling refinements to be made; subsequently allowing for a very reliable comparison between analytical and experimental techniques. It is useful for analytical model verification in the future study.

Thomas J. Boone et al. (1982) performed 10 full-scale experimental tests on double-tee tubular joints made from steel to study the effect of chord axial and bending stresses on the ultimate strength of the joints. Three distinct branch loading conditions were considered by Thomas J. Boone et al. (1982): axial load (four tests); in-plane bending (three tests); and out-of-plane bending (three tests).

3.0 NONLINEAR FINITE ELEMENT ANALYSIS

3.1 Sources of Non-linearity

Nonlinear techniques are employed in the current finite element modeling and analyses. Although linear analysis is a convenient approximation that is adequate for rough design purposes, it is inadequate for sophisticated structural analyses and simulations with material non-linearity, geometric non-linearity and other kinds of non-linearity.

The stress-strain diagram of steel and most metals is approximately linear at low strains, with the elastic modulus defining the constant slope of the material response curve. However, with increasing of strains the slope is not constant anymore and the stress-strain curve becomes nonlinear. Furthermore, beyond the yield point, the strains become partially irrecoverable. At this time, the material stiffness is changing during the loading history and the subsequent structural responses become nonlinear as a result of this material non-linearity. In addition, geometric non-linearity arises when the nature of the problem is such that formulation of equilibrium on the undeformed configuration of the structure is not appropriate. In such cases, phenomenon such as stress-softening and bifurcation of equilibrium may occur.

In summary, both material and geometric non-linearities are considered in the finite element modeling and analyses reported on herein. However, boundary non-linearity is not included.

3.2 Nonlinear Analysis

The nonlinear finite element software package ABAQUS is a multi-purpose engineering analysis software widely used. All of the currently considered finite element models are generated with, and the analyses are performed, utilizing ABAQUS.

In nonlinear analyses, we cannot obtain the solutions by solving only a single system of equations as we do in linear analyses. Instead, the solution is calculated by applying the loading incrementally and solving the problem gradually. To this end, ABAQUS breaks the analysis process into a number of load increments and iterates to find the approximate static equilibrium solution at the end of each load increment until the last load increment from the load history is attained. It often takes ABAQUS several iterations to determine an acceptable static equilibrium solution to a given load increment. The modified Riks-Wempner method is used to solve the nonlinear equilibrium equations related to the modeling considered herein. The Riks-Wempner method is superior to the more commonly used Newton-Raphson method as a result of the former techniques ability to negotiate limit point and capture unstable unloading response in a structure.

The mechanical constitutive models that are provided in ABAQUS consider both elastic and inelastic response. In the inelastic response models, there is a basic assumption that the elastic and inelastic response can be distinguished by separating the deformation into recoverable (elastic) and non-recoverable (inelastic) parts. This separation is based on the assumption that there is an additive relationship between strain rates:

$$\dot{\mathbf{e}} = \dot{\mathbf{e}}^{el} + \dot{\mathbf{e}}^{pl} \quad (3-1)$$

Where $\dot{\mathbf{e}}$ is the total strain rate, $\dot{\mathbf{e}}^{el}$ is the rate of change of the elastic strain, $\dot{\mathbf{e}}^{pl}$ is the rate of change of the inelastic or plastic strain.

The plasticity model employed in the current ABAQUS modeling and analysis is a rate-independent associated flow plasticity model employing the von Mises yield criterion and isotropic hardening.

3.3 True Stress and Logarithmic Strain

When specifying material property parameters in mechanical constitutive models, we must use true stress \mathbf{s}_t and logarithmic strain \mathbf{e}_t . However, material properties are usually offered in the form of nominal stress \mathbf{s}_n and nominal strain \mathbf{e}_n . As a result, we must find a method to convert them into true stress and logarithmic strain. From the ABAQUS user's manual we can find the following developments of the transformation equations.

$$\mathbf{e}_n = \frac{l-l_0}{l_0} = \frac{l}{l_0} - 1 \quad (3-2)$$

$$\frac{l}{l_0} = 1 + \mathbf{e}_n \quad (3-3)$$

where l is the current length, l_0 is the initial length. Then the relationship between logarithmic strain and nominal strain is

$$\mathbf{e}_t = \ln\left(\frac{l}{l_0}\right) = \ln(1 + \mathbf{e}_n) \quad (3-4)$$

Considering the nearly incompressible property of steel material, we have

$$l_0 A_0 = lA \quad (3-5)$$

where A is the current cross-section area, A_0 is the initial cross-section area. The relationship between true stress and nominal stress appears as:

$$\mathbf{s}_t = \frac{F}{A} = \frac{F}{A_0} \cdot \frac{l}{l_0} = \mathbf{s}_n \left(\frac{l}{l_0}\right) = \mathbf{s}_n (1 + \mathbf{e}_n) \quad (3-6)$$

Hence, the equations of transformation from nominal stress and nominal strain to true stress and logarithmic strain are found to be of the form

$$\begin{aligned}\mathbf{e}_t &= \ln(1 + \mathbf{e}_n) \\ \mathbf{s}_t &= \mathbf{s}_n(1 + \mathbf{e}_n)\end{aligned}\tag{3-7}$$

4.0 VERIFICATION STUDY

The experimental tests “Chord Stress Effects on the Ultimate Strength of Tubular Joints” by Thomas J. Bonne, Joseph A. Yura and Peter W. Hoadley (1982) were ultimately selected to serve as the standard against which to assess the robustness of the chosen nonlinear finite element modeling techniques. 10 full-scale experimental tests on double-tee tubular joint specimens were performed to study the effect of chord axial and bending stresses on the ultimate strength of the joints. These tests were selected since the report of Boone et al. provided a great deal of information about the nature and design of the test fixtures, boundary conditions, specimen fabrication, and loading protocols followed. This type of diligent and careful reporting of the details of larger-scale experimental testing is of vital importance to the proper execution of a finite element validation study.

Of the 10 full-scale experimental tests performed by Boone et al. on double-tee tubular joints, two were taken as the focus of the present verification study: test A1 and test AP5.

4.1 Verification Test

4.1.1 Specimens and Test Setup

The geometry details of the specimens are shown in Figure 4.1. The thickness ratio (the ratio of the radius to the wall thickness) of the chord is about 25, and the thickness ratio of the branches is 21.5. The outer diameter ratio of branches to chord is approximate 0.67.

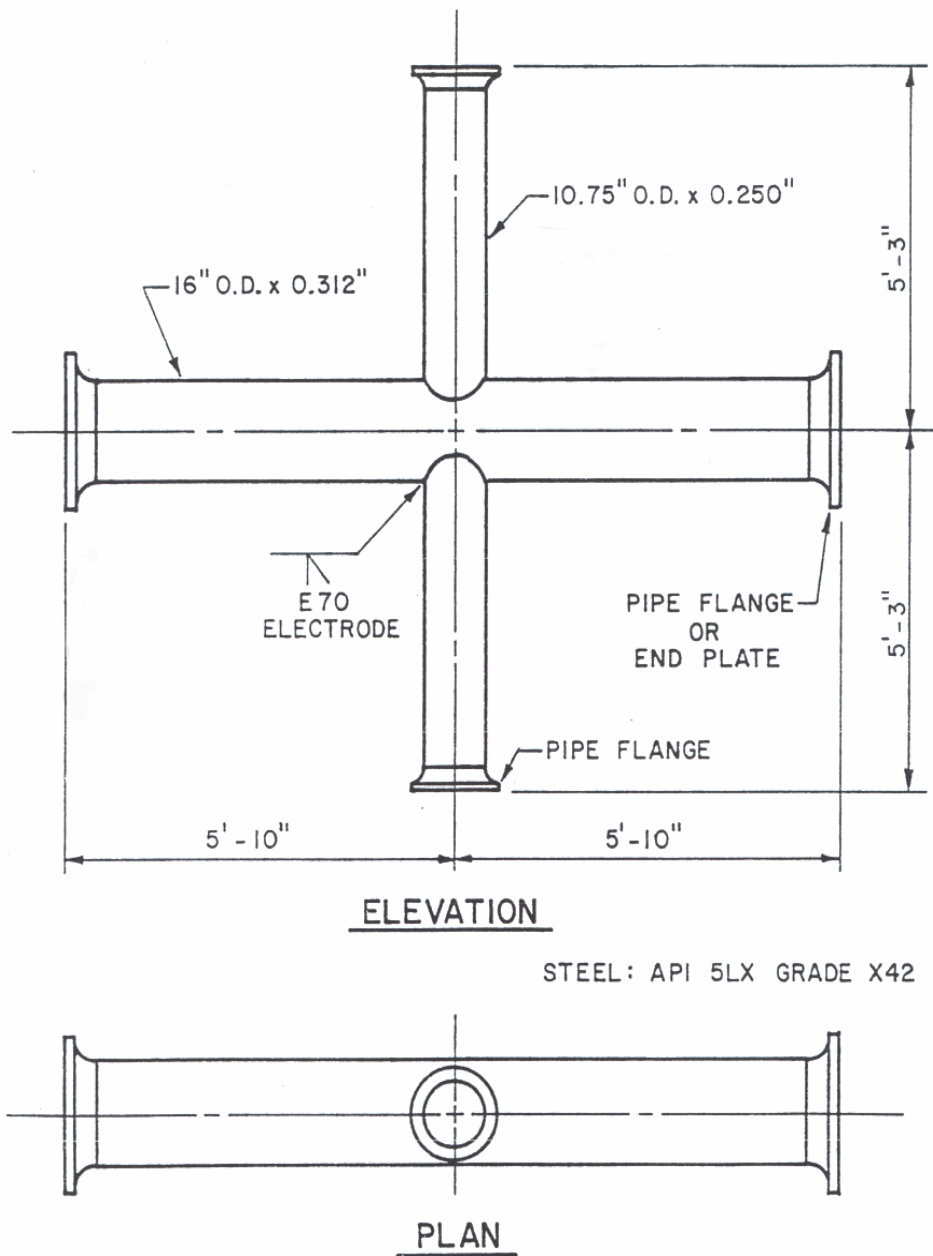


Figure 4.1 Specimen Geometry Details

In order that in-plane bending load actuators and out-of-plane bending load actuators could apply loads to the chord, it was required that the chord centerline be maintained at a constant height relative to the actuator line of action. For the sake of keeping this constant elevation, two 100 kip hydraulic actuators were used: one located between the test frame and the top of the upper branch; and the other located between the end of the lower branch and the floor slab (Boone et al. 1982). The pressure of these two actuators could be controlled as necessary to balance the self-weight of the chord, branches and other test instruments to satisfy static equilibrium while at the same time preserving the chord elevation during the tests. As a result of this loading configuration, the specimen was “floating” in space under the action of the two actuators. Hence care had to be exercised during the testing to ensure that the specimen remained approximately stationary in the vertical direction so that the deflection readings obtained at the branch ends was not contaminated by the rigid body translation of the entire specimen along the branch member longitudinal axis.

In addition, four 200 kip center hole actuators and four 2-inch-in-diameter high-strength steel rods were used to apply axial forces to the chord. The actuators were installed on plates at the ends of the chord. The rods passed through the chord and were positioned at each end by holes in the chord end plates also. During the process of applying axial forces, the chord end plates transferred the compression load from the tension rods to the chord wall.

In terms of the boundary conditions employed in the experimental testing, Boone et al. went to great lengths to ensure that ideal pinned conditions were present at both the top and bottom of the cruciform specimens at the ends of the branch members. The chord member was constrained by the test set-up so that out of plane translation and rotation about the longitudinal

axis of the branch members were prohibited. These boundary conditions were duplicated in both specimens of test A1 and test AP5.

Coupon tests were performed to get the material properties. The tensile yield strength of the chord was determined to be 46.6 ksi, and that of the branch as 48.0 ksi. And the compressive yield strength of the chord is taken as 44.5 ksi, and that of the branch as 44.4 ksi; these latter values were determined using the 0.2% offset method.

4.1.2 Instrumentation

The primary objective of all the tests was to establish the ultimate tubular joint capacity for the branch axial load. All the loads were monitored using a pressure gage accurate to 25 psi and a pressure transducer accurate to 0.25%. The branch axial loads were considered accurate to ± 0.2 kips. The chord load levels were considered accurate to ± 1 kips.

The primary deflection measurements were monitored with mechanical dial gages accurate to 0.001 in. and linear voltage displacement transducers; both had a 2 in. stroke. The location of all the dial gages and inclinometers are shown in Figure 4.2. Since the whole specimen might move vertically during testing, dial gage 3 and dial gage 4 were used to determine the possible rigid body motion of the chord center. The average of these two gages, which showed the rigid body vertical motion of the chord, was utilized to modify the deflection of the upper and lower branch ends. (Boone et al. 1982)

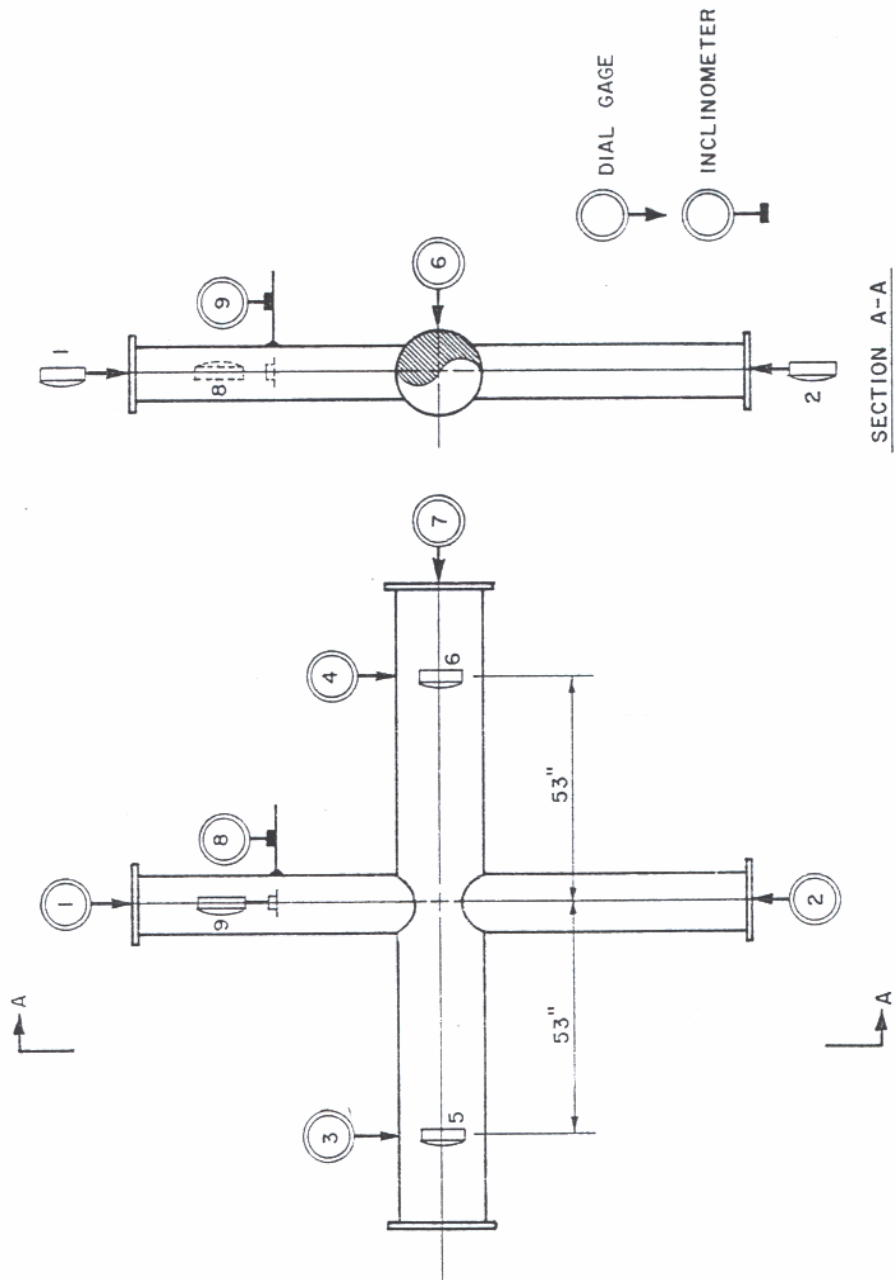


Figure 4.2 Location of Dial Gages and Inclinometers

4.1.3 Tests

Only two out of the ten full-scale double-tee tabular joints experimental tests were considered in the current verification study: test A1 and test AP5. Test A1 involved the application of axial loading, along the entire circumference of the tube walls occurring at the ends of the branch (vertical) members, in the absence of chord loading. Figure 4.3 displays a schematic of the loading condition associated with this test specimen. Test AP5 was identical to test A1 in all respects except that the chord member was loaded with a concentrated compressive force applied on the end plate and then distributed around the circumference of the tube wall (as shown schematically in Figure 4.3). The distributed chord stress was $0.6 F_y$, where F_y is the average tensile yield strength from the chord coupon tests.

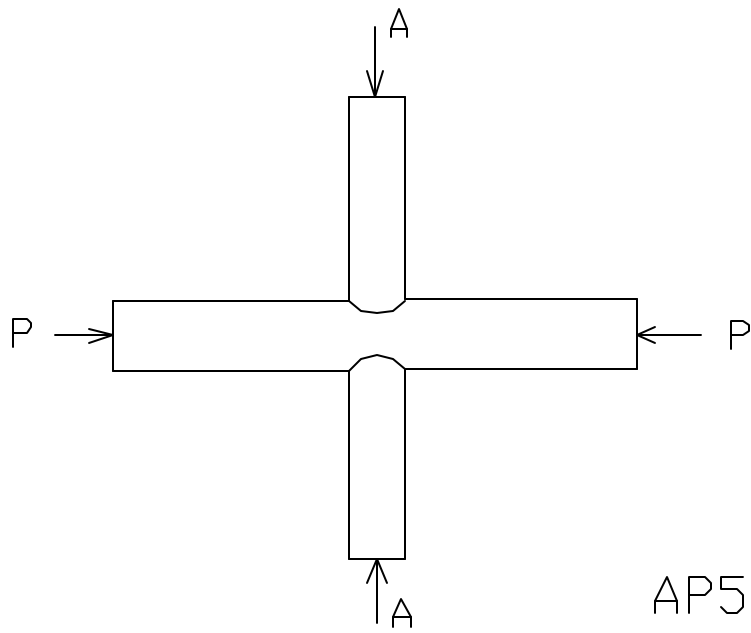
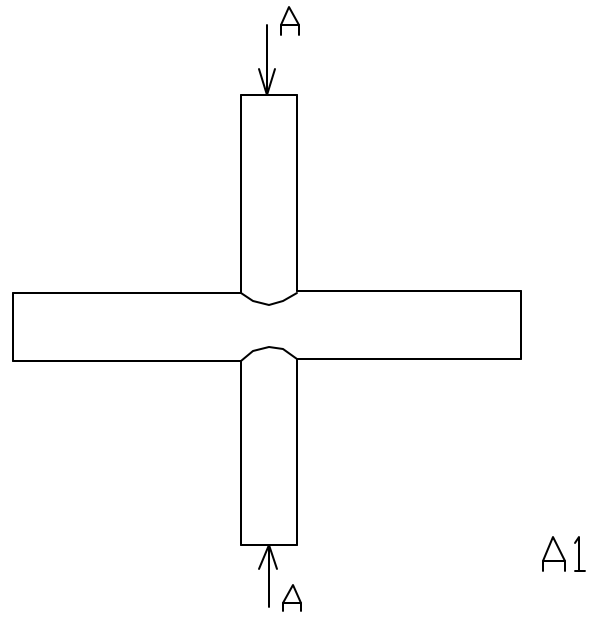


Figure 4.3 Elevation View of Experimental Branch Specimen A1 & AP5

4.2 ABAQUS Modeling

When constructing the finite element meshes of the models used in the verification study focusing on test A1 and test AP5, a dense mesh of nonlinear shell finite elements (S4R) is used to replicate the actual three-dimensional geometry of the specimens. The shell elements are positioned to coincide with the middle surface of the hollow structural sections.

The employed S4R shell element is a kind of nonlinear, finite strain, shell element from the ABAQUS element library. ABAQUS provides shell elements that allow the modeling of curved, intersecting shells, which can present nonlinear material response and undergo large overall motions, translations and rotations. S4R shell element is a kind of general-purpose shell element, which provides powerful and accurate solutions in all loading conditions for thin and thick shell problems (ABAQUS 2001).

The resulting meshes consist of: 1) for the chord, 140 elements along the 140” length, and 48 elements around the circumference with the mid-diameter of 15.688”; and 2) for one of the branch, 75 elements along the 63” length, and 44 elements around the circumference with the mid-diameter of 10.5”.

The ends of the test specimens, both chord and branches, were equipped with pipe flanges or end plates, and had larger stiffness than open tubes. In order to consider this boundary condition, the MPC (multi-point constraints) command was used at the ends of the chord and branches in the nonlinear finite element models. The MPC type BEAM provides a rigid beam between two nodes to constrain the displacement and rotation at the first node to the displacement and rotation at the second node, corresponding to the presence of a rigid beam between the two nodes. (ABAQUS 2001) By defining the ends of centerlines of tubes as the master nodes of the rigid beams, and the nodes around the perimeter at the end of tubes as slave

nodes of the rigid beams, the ends of tubes can move and rotation according to the displacement and rotation of the end centers and thus the condition of a rigid welded plate on the tube end is duplicated.

In the finite element models, an ideal pinned condition is imposed at the bottom branch member end. At the top branch member end, an ideal roller condition is imposed, thus allowing for the vertical axial shortening of the branch member under the action of the imposed force. In the chord member, only out-of-plane displacement is constrained at the member ends. Such chord member constraint is useful for duplicating test conditions as well as for ensuring that the finite element model is not unstable due to rigid body rotation about the branch member longitudinal axis. Only the upper branch end is loaded; the bottom branch end is ideally pinned. This last point is a deviation from the experimental procedure followed by Bonne et al. since the finite element model does not have to contend with the presence of the rigid body translational mode along the branch member longitudinal axis, which existed in the experimental test specimens.

Boone and his co-workers went to great lengths to properly record the initial global imperfections present in the fabricated double-tee specimens. They provided the initial out-of-plane and in-plane alignment of the branches. As a result, it is possible to incorporate these initial displacements into the finite element models as perturbations to the perfect geometry obtained through the ABAQUS pre-processing routines.

The axial compression force applied to the chord is achieved by imposing a concentrated force on the master node of MPC type BEAM (i.e. the end of centerline of the tube). Distributed forces are then imposed on the nodes of the elements around the perimeter of the hollow

structural section (i.e. the slave nodes of the BEAM MPC). The resultant force equals the equivalently applied experimental loading, which is

$$0.6 \times 46.6 \times \mathbf{p} \times (16^2 - (16 - 0.312)^2) \div 4 = 421.8 \text{ kips} \approx 422 \text{ kips}$$

Furthermore, the summary of results from the material testing program discussed in the final report of Boone et al. allowed for the formulation of a constitutive law used in the modeling that was representative of the material properties present in the test specimens. The known relationships between nominal stress and true stress, and between nominal strain and true logarithmic strain are used to get the constitutive law used in finite element verification studies (see Chapter 3 for the equations). The plot for true stress versus logarithmic strain is shown in Figure 4.4.



Figure 4.4 Constitutive Law Used in Finite Element Verification Studies

4.3 Study of Results from Experiments & ABAQUS

4.3.1 Results Comparison

In all cases, the agreement between predicted finite element ultimate strength and experimentally observed ultimate strength is less than 4.0 percent.

Table 4.1 Comparison of Result from Tests and ABAQUS

	Ultimate Strength (kips)		Difference
	Experimental	ABAQUS	%
A1	78.8	75.65	4.0
AP5	57.9	56.71	2.1

Plots of the load-deflection response from both experiments and ABAQUS for the analogs of test A1 and test AP5 are presented in Figure 4.5 and Figure 4.6. For the experimental load-deflection curve, the load represents the axial forces read from the lower actuator and the total deflection is two times the deflection at the far end of the lower branch. For the case of the load-deflection curve from the nonlinear finite element analysis, the load is the force applied on the upper branch and the total deflection is the displacement of the upper end of the upper branch versus the far end of the lower branch.

Deformed geometries of the two specimens and the associated finite element analogs are presented in Figure 4.7 and Figure 4.8 for specimen of test A1, and in Figure 4.9 and Figure 4.10 for specimen of test AP5.

Generally, good agreement is observed to occur when comparing the finite element model results with the experimental results. On the whole, the finite element models tend to slightly under-predict the ultimate strength of the double-tee assemblies. Furthermore, the finite

element models tend to predict a stiffer response in the elastic range than what was reported by Boone et al. This last observation is most conspicuous in the test A1 verification results presented in Figure 4.5. Here the significantly stiffer finite element results are quite apparent as compared with the experimental results.

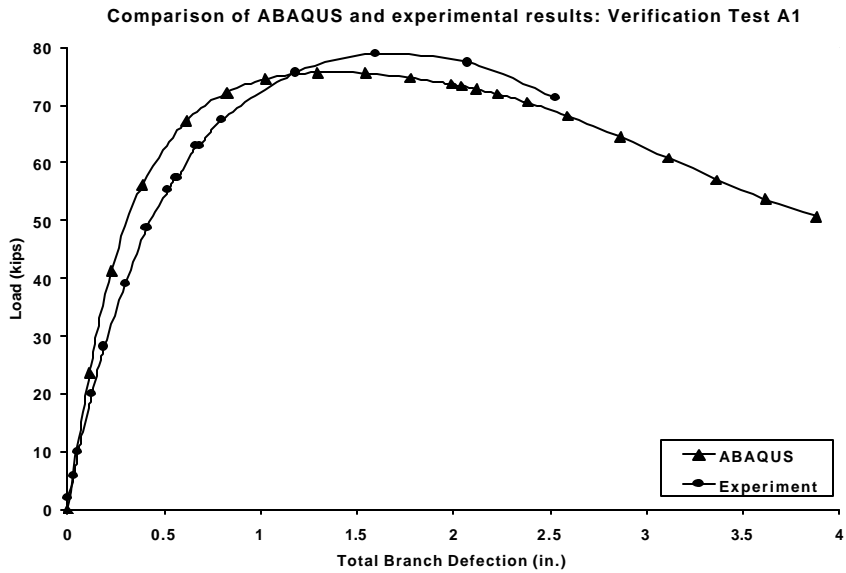


Figure 4.5 Comparison of ABAQUS and Experimental Results: Test A1

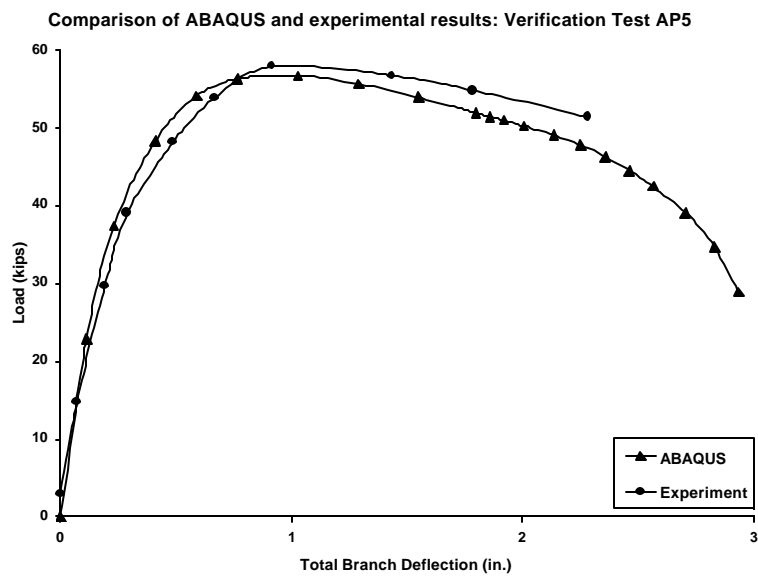


Figure 4.6 Comparison of ABAQUS and Experimental Results: Teat AP5

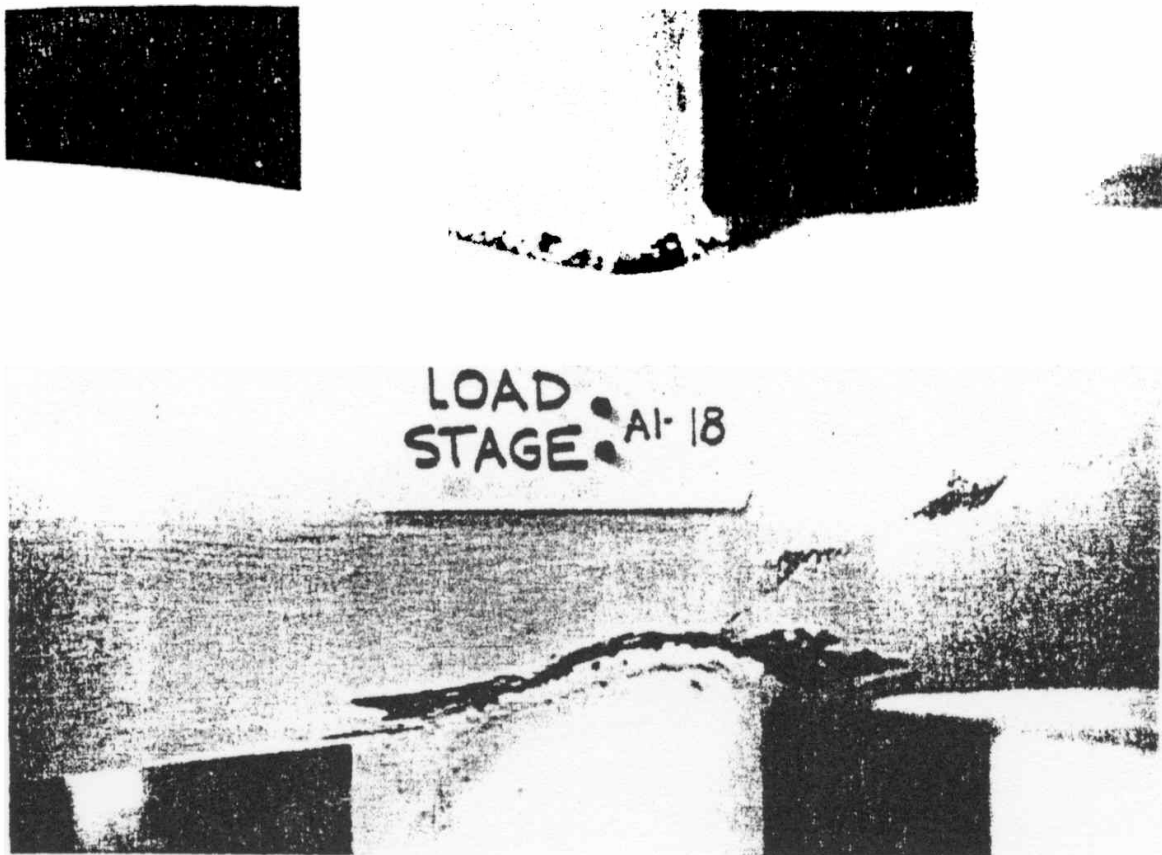


Figure 4.7 Deformed Geometry of Specimen A1 from Experimental Testing

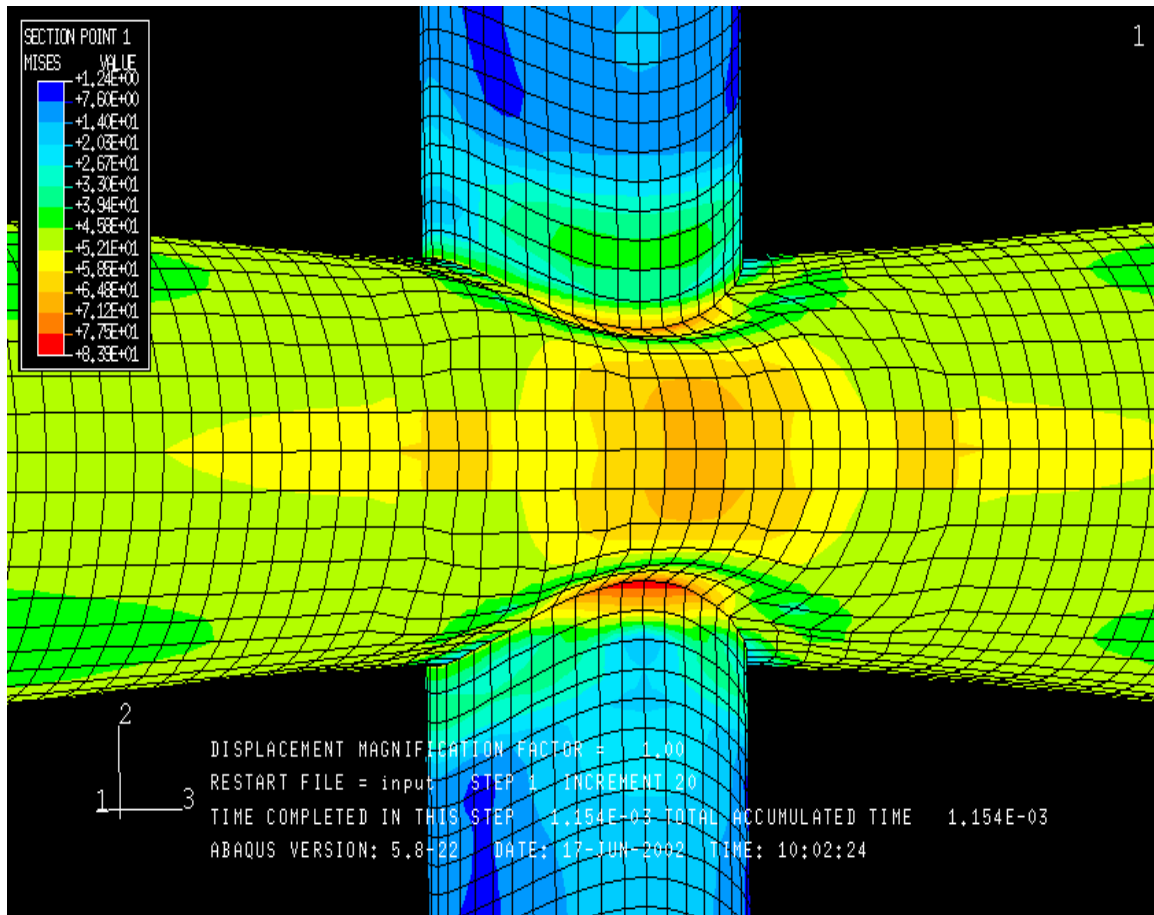


Figure 4.8 Deformed Geometry of Specimen A1 from ABAQUS



Figure 4.9 Deformed Geometry of Specimen AP5 from Experimental Testing

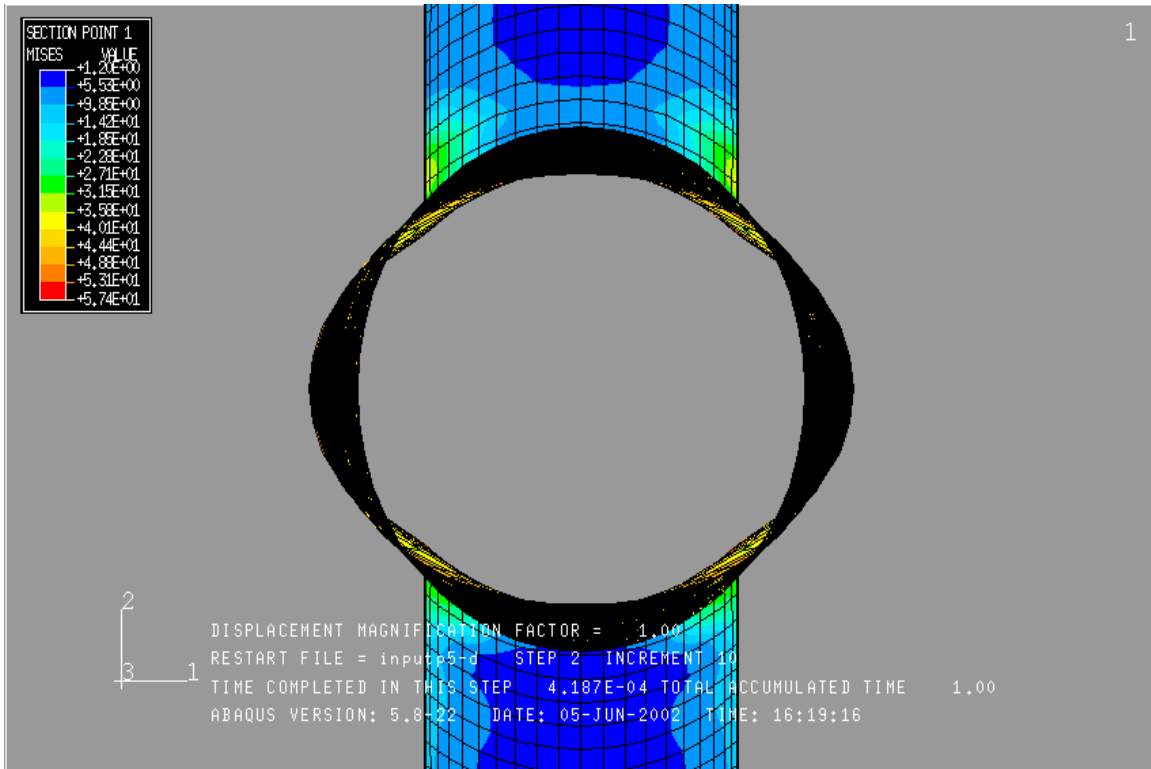


Figure 4.10 Deformed Geometry of Specimen AP5 from ABAQUS

Bonne and his co-workers carefully recoded the initial global imperfections of the branches. Besides considering these imperfections, an ABAQUS model without the global imperfections (i.e. using the perfect geometry obtained through the ABAQUS pre-processing routines) was also considered. Plots of the load deflection responses of models with both perfect geometry and imperfect geometry are presented in Figure 4.11. The load-deflection curve obtained from the model with perfect geometry shows almost same elastic stiffness as the model incorporated with imperfection. Moreover, with the increase of axial load in the branches, the load-deflection curves of perfect case exhibits stiffer response and obtains higher ultimate strength.

Further investigations into the important features of the finite element modeling reveal the need for consideration of the end stiffening plates on the chord members. In the accordance with the experimental tests considered in the verification models, MPC type BEAM elements are used in the ABAQUS models, and the axial forces are applied at the master nodes of these elements (i.e. the centers of the end planes). Hence, the perimeter at ends of the chord maintain in a perfect circular geometry throughout the load history. Besides simulating the chord ends according to actual boundary condition, an ABAQUS model of another case was studied: letting the ends of the chord freely deform without multi-point constraints, and only constraining the out of plane displacements of every node around the perimeter at the ends. Hence, the ends of the chord were much softer than in the former case. The load-deflection curves of the analogs of test A1 are showed in Figure 4.12. Here we can see, the load-deflection curve obtained from the case without the MPC type BEAM at the ends of the chord display almost same elastic stiffness as that with MPC elements. However with increasing the load, the load-deflection curve of the model with the MPC BEAMs displays a larger stiffness and attains a higher ultimate load.

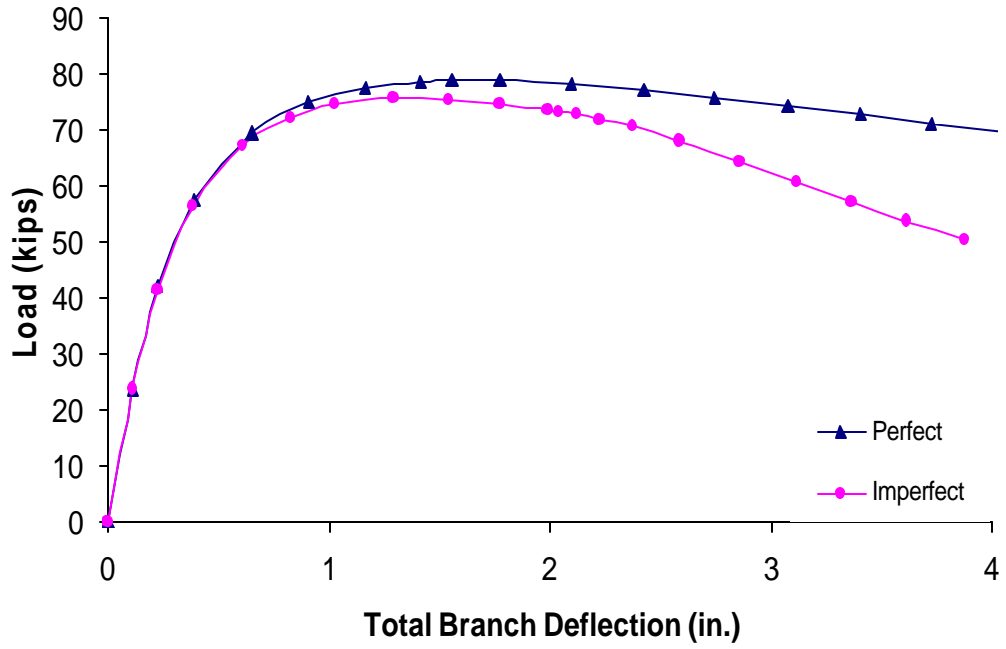


Figure 4.11 Comparison of Models with Perfect and Imperfect Geometry

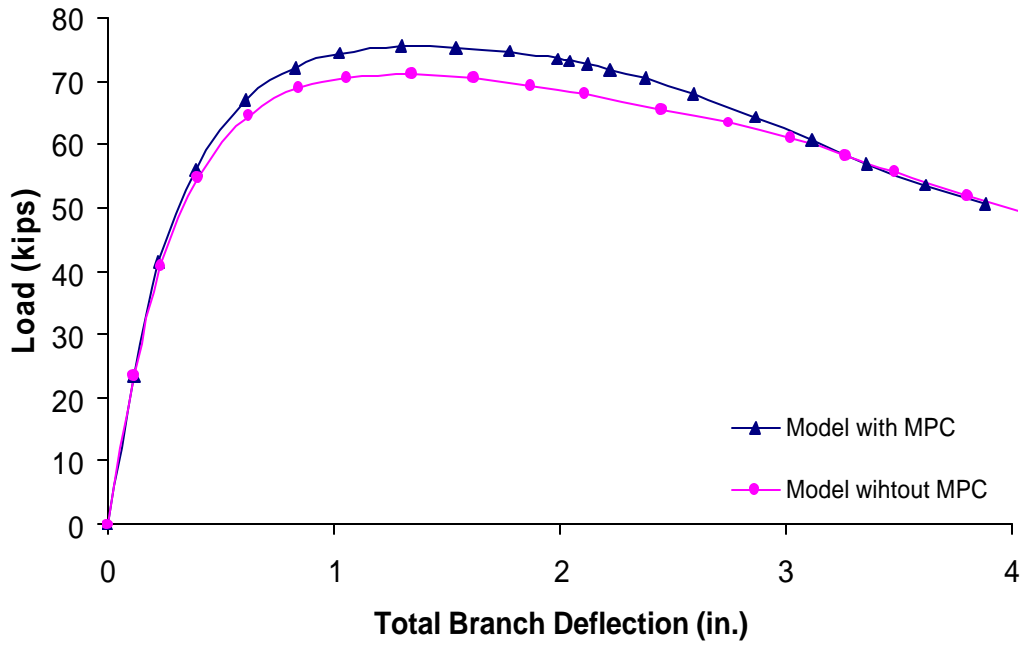


Figure 4.12 Comparison of ABAQUS Models with MPC and Without MPC

4.3.2 Discussion of Comparison Results

In the pursuit of the root cause for the apparently overly stiff response of the finite element models, imperfection fields with very large magnitudes are tried in order that the modeling response might be softened. Even after incorporating unrealistically large imperfections, the finite element method results are still stiffer than the experimental results. Furthermore, attempts are made to vary the material model parameters used in the finite element modeling so as to improve agreement between the modeling and experimentation. Since the less than ideal agreement between the experimental and finite element method results is apparent in the initial load-deflection slope, the elastic modulus of the steel has the greatest impact on the response. Pursuing this notion, the elastic modulus of the model is reduced significantly in an effort to try and improve agreement between the finite element and experimental results. What is found is that the elastic modulus has to be reduced far below that, which is characteristic of steel, before any improvement in results could be discerned. In addition to the above measures, an investigation of the modeling response as a whole is undertaken so as to identify any mathematical anomalies that might be manifest in the models as a result of the element formulations used. Specifically, no evidence of shear locking or membrane locking is apparent within the models.

As a result of the foregoing efforts, it becomes clear that the modeling strategies employed should be sufficient to properly model the response of the double-tee specimens considered (especially within the linear-elastic response domain). Based on this conclusion, an assessment of the experimental techniques employed in the study of Boone et al. is made. It appears that the lack of agreement between the observed initial specimen stiffness most likely emanates from the means used to support the specimens during testing and is mostly likely

attributable to the experimental procedure rather than an underlying shortcoming in the finite element techniques employed.

As mentioned earlier in our discussion on the boundary conditions employed in the experimental modeling, the specimens were not positively anchored to a load frame or reaction floor during testing. Rather, the double-tee specimens were supported at their branch ends by one actuator each, exerting a force along an axis coincident with the branch longitudinal axis. As a result, the specimens were permitted to “float”, to some extent, within the load frame. The only means to guard against excessive deviations in the specimen rigid body motion was manual control of the actuators governed by the operator’s observations of two dial gauges placed on the chord member. The dial gauges were placed on the top wall of the tubular chord member with the intent that any excessive “floating” of the specimen would be perceived through a shift in the dial gauge readings. This method of reckoning is quite imperfect since the local deformations of the tube wall cannot be separated out from the dial gauge readings (i.e. local deformations were additive with whatever rigid-body translation occurring). Similarly, by relying on manual means to adjust actuator forces, so as to bring the observed deviation in the dial gauge measurement back to the null value, significant errors could be introduced as a result of stress relaxation as well as human error. Based on these observations, it is felt that perhaps the deviation between the slopes of the initial load-deflection response of the experimental and finite element specimens is not as important as first thought.

4.4 Conclusion

After carefully studying the modeling approach employed, as well as the influence of imperfection fields of differing magnitudes, as well as the effects of material constitutive modeling on the finite element results, the validity of the modeling results is supported. Based on the foregoing, it is believed that the finite element models are furnishing physically meaningful results comparable to those obtained through experimental testing. The techniques used in the verification study have been employed during the remainder of the present research.

5.0 WTEE BEARING MODEL

Based on the results from the verification study of the non-linear finite element modeling techniques reported on in Chapter 4 of the current thesis, it appears that the proposed modeling techniques are adequate for use in the current research. The present chapter is focused on the study of connection response in large diameter circular hollow structural sections, connection details that are typical in long-span tri-chord sign structures.

5.1 Statement of Problem

The regions of the circular chord HSS and WTEE upright that are immediately adjacent to the chord-column connection region are the focus of this portion of the research. From the Design Tables of Loading Type-1 for overhead sign structures used by Commonwealth of Pennsylvania Department of Transportation (BD644M), two critical cases were identified as the focus for further study.

Spans of tri-chord trusses range from 18,000 *mm* to 72,000 *mm*, the latter value being employed for the HSS chord length in the ABAQUS model. The outer-diameters of chords range from 127 *mm* to 660 *mm*. Once again, the largest diameter (660 *mm*) is selected as the outer-diameter of the HSS chord so as to create a “worst case” condition. For the given 660 *mm* diameter, the wall thicknesses are varied between 9.62 *mm* and 12.7 *mm*.

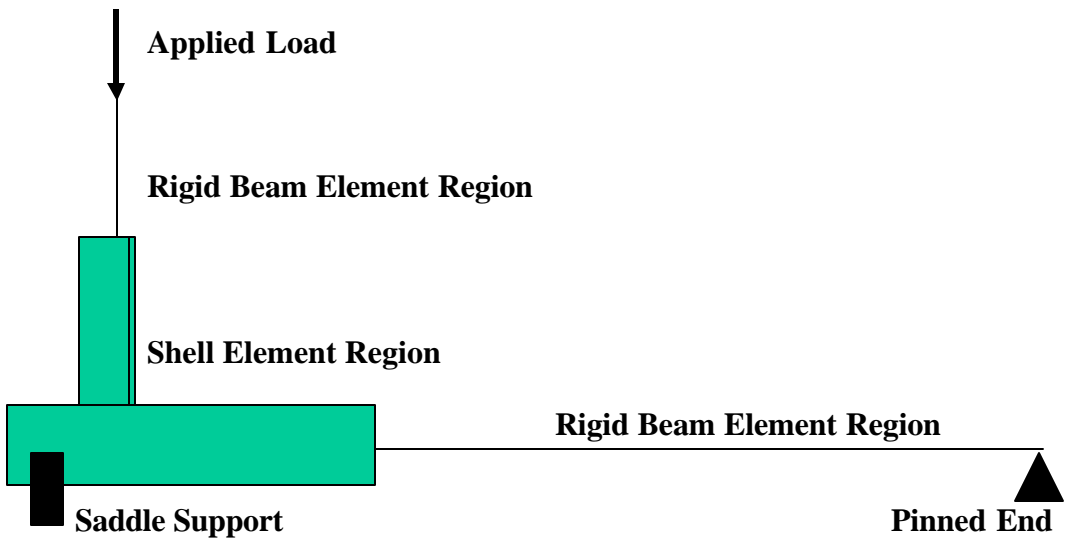
In both cases, the WTEE used is an ST255 ? 71.5 structural element. The length of the WTEE that is pin-pin connected to the chord in a tri-chord sign structure is

$$\text{Span}/23 - \text{HSS Diameter} = 72,000/23 - 660 = 2,530.4 \text{ mm} \approx 2,500 \text{ mm}$$

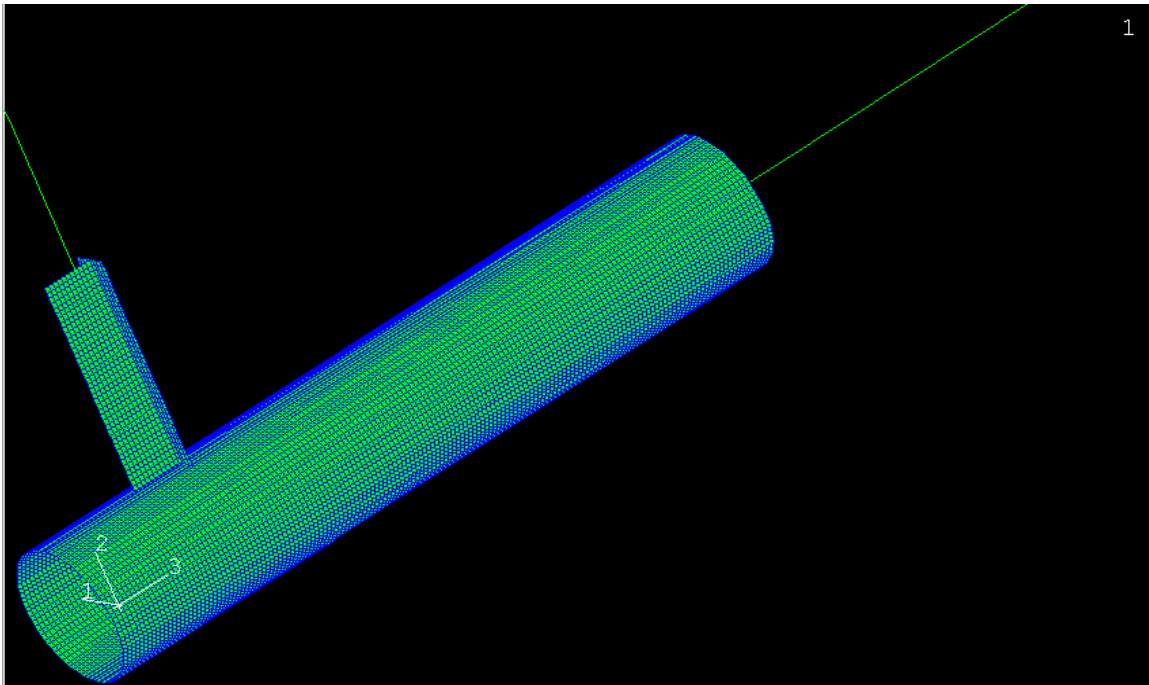
In order to avoid a local crushing failure at the ends of the chord in bearing with the supports, saddles having curved bearing surface, in accordance with the curved outer surface of the chord (see Figure 1.4), are employed to increase contact area at the chord end. The length of the saddle along the longitudinal dimension of the chord is 300 *mm*, and the depth of the concavity is 204.8 *mm*. The center of the saddle is 225 *mm* away from the end of the chord.

5.2 WTEE Bearing Model

Figure 5.2 presents a schematic of overall geometry and loading of the nonlinear finite element WTEE bearing model. The focus of the analysis is the joint through which the axial force acting in the upright WTEE member is transferred to the circular HSS sidewall. The chord-WTEE intersection regions are modeled in a detailed way using dense meshes of four-node nonlinear shell finite elements, S4R (ABAQUS 1999), positioned at the mid-plane of the constituent plate components making up the cross-sections in question. In other words, only portions of the HSS chord and WTEE are modeled in detail with shell finite elements.



(a) Schematic of WTEE Bearing Model



(b) Overview of WTEE Bearing Model

Figure 5.1 Overall Geometry and Loading of WTEE Bearing Model

In the case of the HSS chord, a length of more than five times the diameter of the tube, or $3,525\text{ mm}$, is modeled explicitly with shell elements; while in the case of the WTEE, a length of nearly four times the cross-sectional depth, or $1,000\text{ mm}$, is modeled with the shell elements (as measured up from the HSS-to-WTEE connection). These distances are felt to be adequate from the standpoint of applying St. Venant's principle related to the small influence that far away material has on the local state of stress at a definite location. The remainder of the member lengths of the HSS and WTEE are modeled using two-node nonlinear beam elements, B33.

The B33 beam element is a one-dimensional line element in three-dimensional space that has stiffness associated with deformation of the line. It's one kind of Euler-Bernoulli beams, which are used to model slender beams that do not allow for transverse shear deformation (ABAQUS 2001).

In the case of the HSS, three beam elements comprise the left $68,475\text{ mm}$ portion; while in the case of the WTEE, two beam elements make up the left $1,500\text{ mm}$ portion. The resulting overall length of the circular HSS (shell elements plus beam elements) is $72,000\text{ mm}$ and the overall length of the WTEE is $2,500\text{ mm}$ (shell elements plus beam elements). The circular HSS chord sizes considered in this study are: case 1 – $660\text{ mm} \times 9.52\text{ mm}$; and case 2 – $660\text{ mm} \times 12.7\text{ mm}$, both sets of values are given in outer-diameter \times wall thickness format.

Compatibility in displacements and rotations at the transition interfaces between the shell elements and beam elements is achieved by enforcing Navier's plane-section hypothesis with constraint equations applied with the MPC command. The boundary conditions on the circular HSS consists of a single pin at the last node of the beam element on the far-end (i.e. the end away from the connection), and pins applied to every node around the circumference of the HSS

in contact with the required saddle as called out in BD-644M. A single concentrated load directed towards the HSS is applied to the last beam node of the WTEE member.

Mild steel, of grade 250, is applied to all components. A plot of the material model, or constitutive law, used is presented in Figure 5.3.

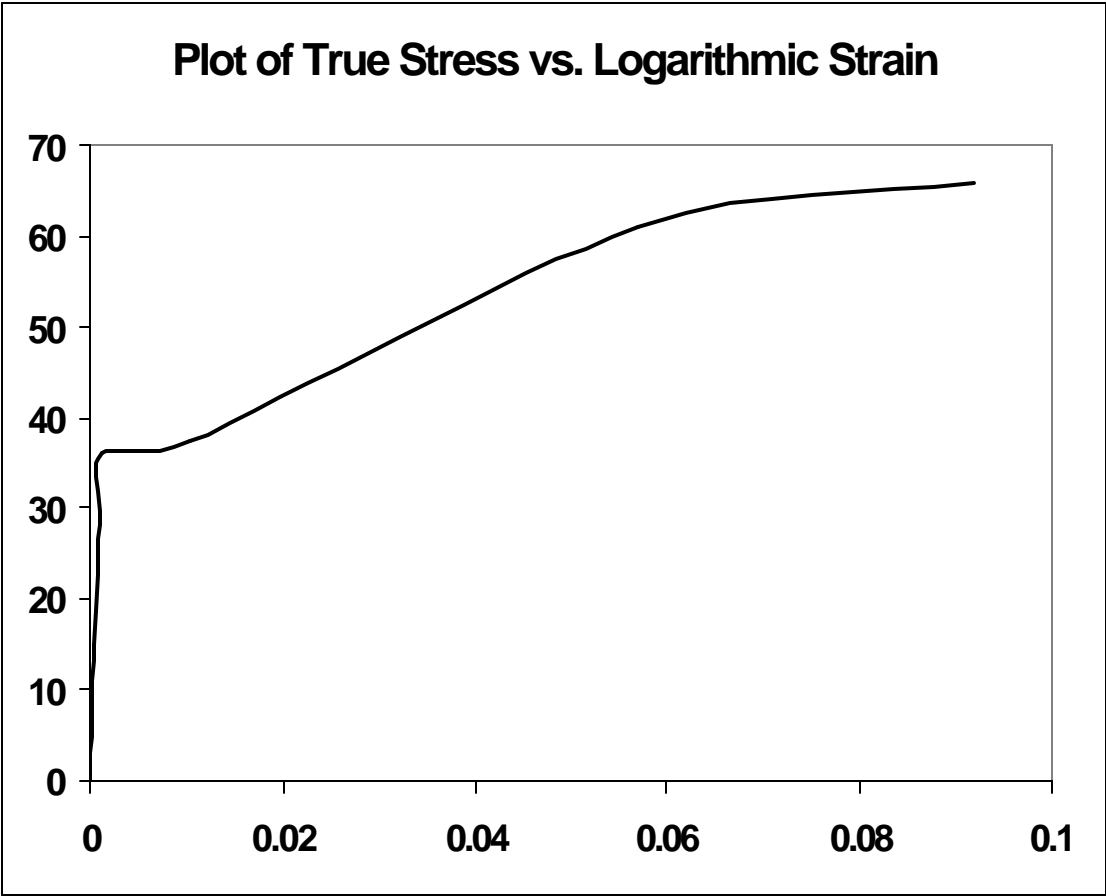


Figure 5.2 Constitutive Law Used in WTEE Bearing Model

5.3 Results from WTEE Bearing Model

From the .STA File, to which ABAQUS writes incremental solution status data during analyses, we can get the bearing capacity of the hollow structural chord transversely loaded by the structural WTEE. For example, the reference magnitude for concentrated load is $4 \times 10^6 N$ (see Appendix A: Input File of WTEE Bearing Model) and the maximum value of the Load Proportionality Factor (LPF) is 0.0421 (Appendix B: .STA File of Case-1). Hence, the bearing capacity in the case with chord wall thickness of 9.62 mm is:

$$4 \times 10^6 \times 0.0421 = 168400N$$

While in the case with chord wall thickness of 12.7 mm, the LPF is 0.0760 (Appendix B: .STA File of Case-2). Therefore the WTEE bearing capacity from ABAQUS analysis is

$$4 \times 10^6 \times 0.0760 = 304000N$$

The use of MPC type BEAM is used to satisfy compatibility between shell and beam elements at the transition interface between the two types of elements. The MPC type BEAM actually adds some constraint to both the HSS member and WTEE members. With the multi-point constraints, the perimeter of the chord at the transition interface maintains in a perfect circular geometry throughout the load history. In fact, we know that the perimeter of the chord can deform freely in actual sign structure installation and hence such installations are expected to exhibit a response that is somewhat softer than that of the models with MPC constraints. Since more constraints are applied to the chord, the true bearing capacity should be a little smaller than that predicted from the ABAQUS model. However, from the St. Venant's principle, we may

ignore the difference since the connection of dense shell mesh and the mesh of beam elements is far from the WTEE connection region.

The stress distribution of the failure mode is exhibited in Figure 5.4 and Figure 5.5.

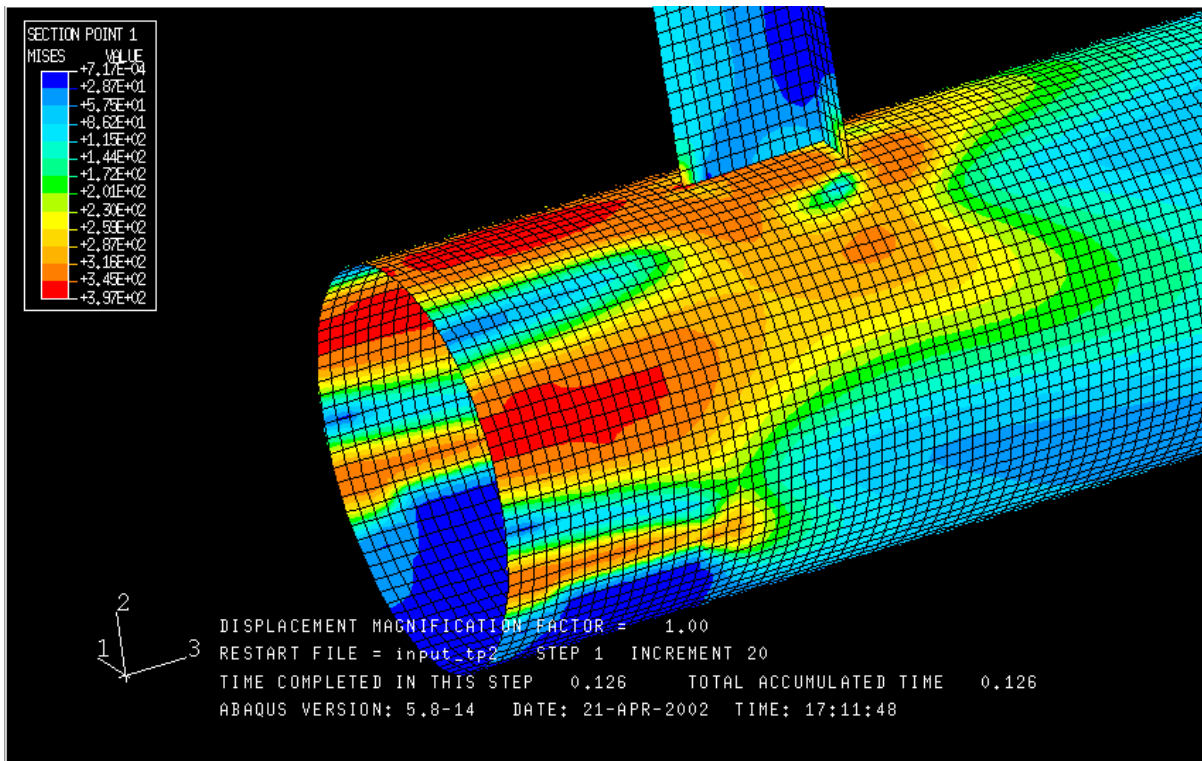


Figure 5.3 Representative Yield-Line Formation in WTEE Bearing Model -1

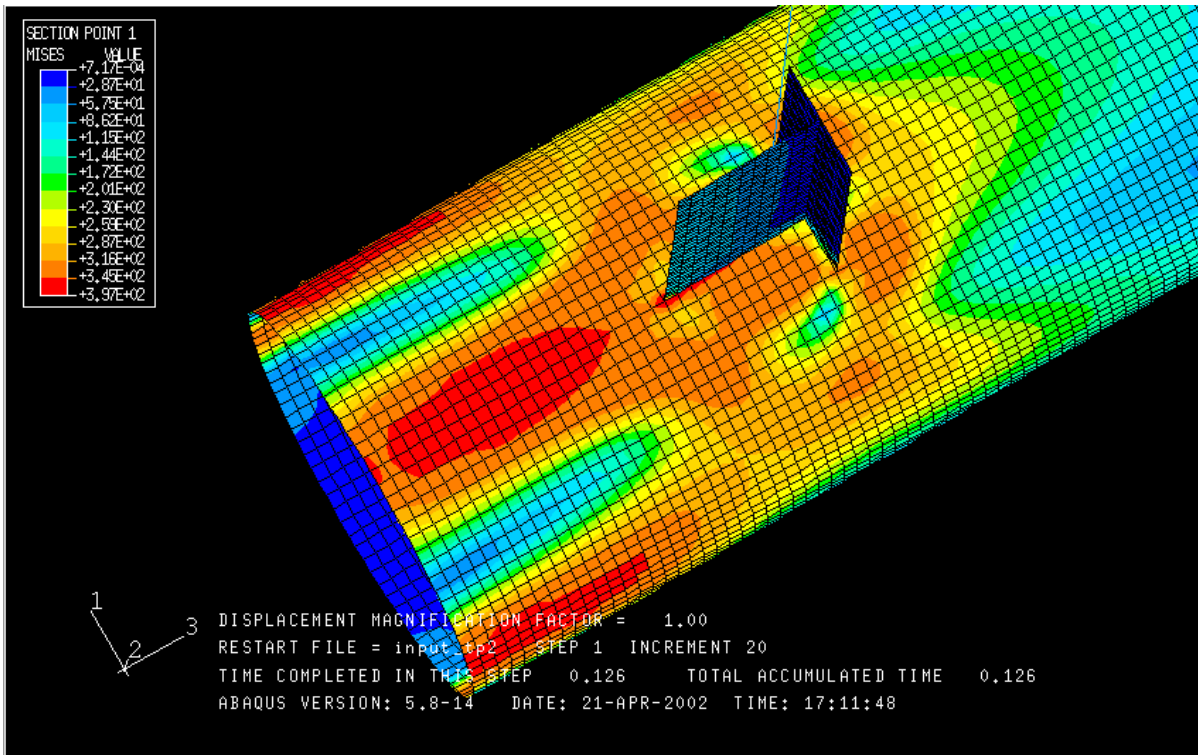


Figure 5.4 Representative Yield-Line Formation in WTEE Bearing Model -2

6.0 WTEE BEARING CAPACITY ESTIMATION

The objective of the current portion of the research is to provide a recommendation for assessing the bearing capacity of the circular hollow structural chord section acted upon by a transverse concentrated load transmitted to the chord sidewall by a WTEE rolled section.

6.1 Estimation of WTEE Bearing Capacity

6.1.1 Assumptions and Approximations

Based on careful observations associated with the nature of the governing failure pattern of specimens, as manifested in the connection region (see Figure 5.4 and Figure 5.5), it is decided that a useful and simple closed form equation (suitable for design office use) might be arrived at through an energy balance approach applied with the Upper Bound Theorem from the theory of plasticity. Such an approach is applied to a yield-line based mechanism whose geometry and kinematics are consistent with observed features in the finite element specimen failures.

To this end, several approximations, related to geometry, loading and yield-line trajectory, are incorporated into the energy approach so as to simplify the mathematics. For instance, instead of a “T-shaped” loading being applied to the tube, it is assumed that a load “ w ” is uniformly distributed along the web only (i.e. a uniformly distributed load acting along the WTEE web, parallel with the HSS longitudinal axis is used) and extended to the end of the chord. Furthermore, despite the fact that the yield lines in the circular HSS sections analyzed with ABAQUS seem to display inclined trajectories with respect to the HSS centerline, they are assumed to be parallel to the centerline in the energy balance equation. The final assumption in the design equation approximation is that the circular HSS is only of length “ d ”; where “ d ” is

defined to be the length from the connection end of the HSS to the top of the WTEE flange as shown in Figure 6.1.

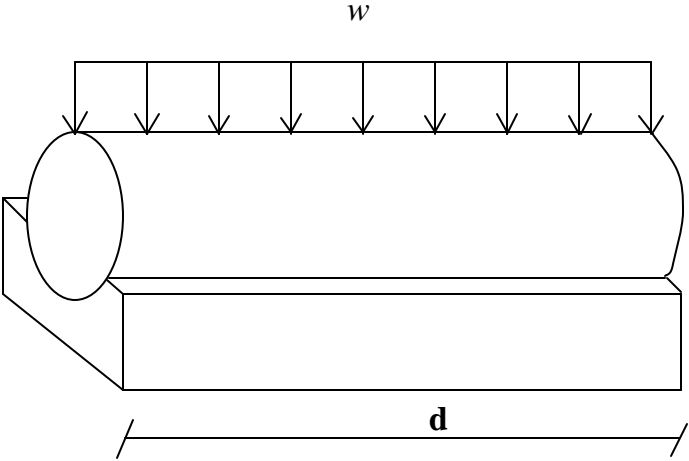


Figure 6.1 Bearing Capacity Estimation Model

It is assumed that the collapse mechanism is formed by five yield-lines: one top yield line on the upper wall of the HSS, two lower yield lines near the extreme edges of the saddle, and two mid yield lines at the mid-height of the upper yield line and the lower yield lines (please see Figure 6.2). So, the HSS is divided by the yield lines into several curved portions that are treated as planes in the analysis procedure. The straight lines in the figure graphically depict these planes (e.g. AB and BC). As a result of these simplifications, the design formulation process is greatly simplified.

6.1.2 Deducing the Estimation Equation

Figure 6.3 shows us the detailed geometry of the chord cross section. The solid lines represent the initial geometry of the HSS and the dashed lines represent the geometry of the failure mechanics.

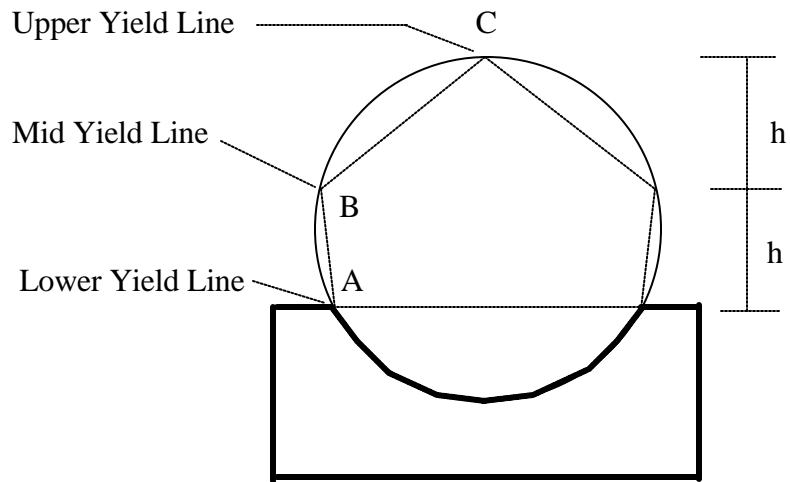


Figure 6.2 Yield Lines of HSS Mechanism

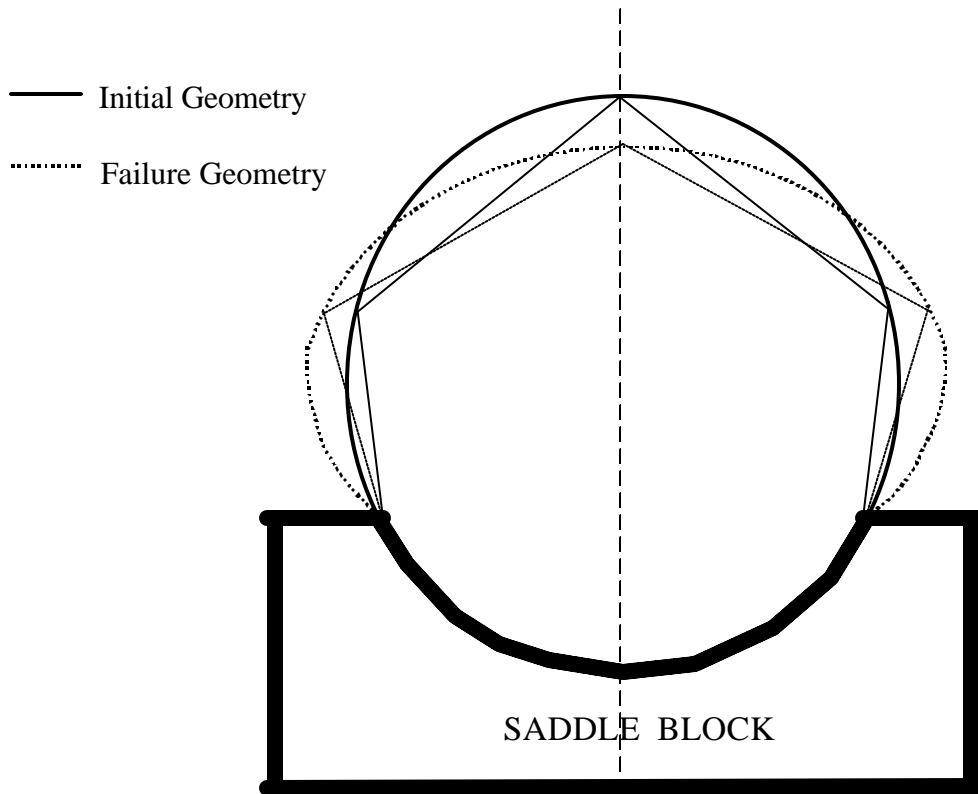


Figure 6.3 Detailed Initial & Failure Geometries of HSS Mechanism

Since the geometry and loading are symmetrical and there are no displacements in the lower part of the chord, we can simplify the calculation model as that shown in Figure 6.4 with half cross section and half loading $w/2$.

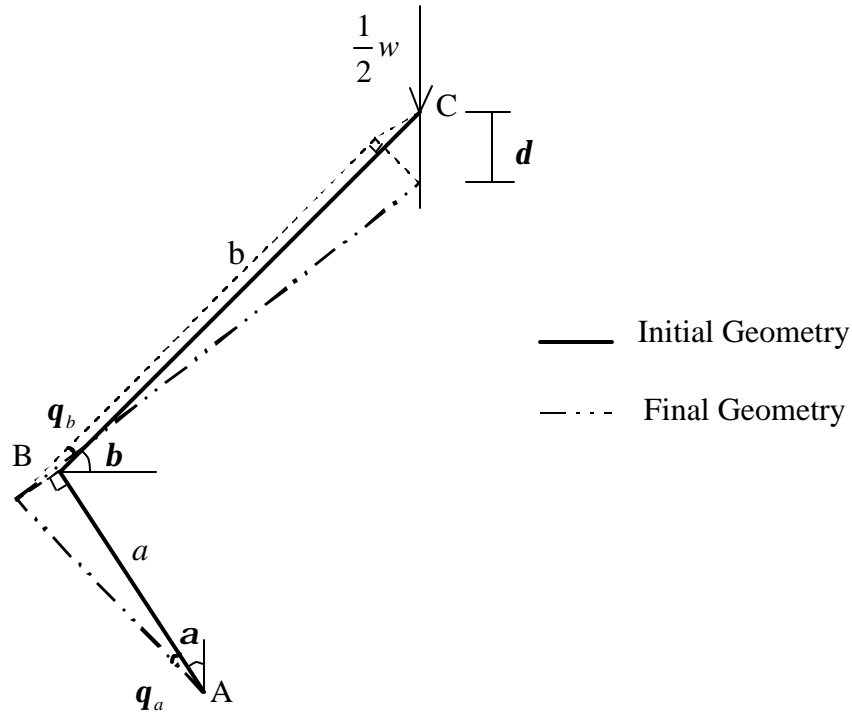


Figure 6.4 Simplified Mechanism Model

According to the Upper Bound Theorem (Chakrabarty 1987), the actual bearing capacity is always less than or equal to the predicted load obtained by equating the external work done by the uniformly distributed load to the internal work absorbed at the yield lines in our proposed failure mechanics.

The external work done by the half of uniformly distributed load w is

$$\frac{1}{2} w \cdot d \cdot d$$

Here, “ d ” is the infinitesimal vertical displacement of the top wall.

We define θ_a as the infinitesimal rotational angle of AB and θ_b as the infinitesimal rotational angle of BC. So, the rotation at the upper yield line is θ_b , the rotation at the lower yield lines is θ_a , and the rotation at the mid-yield lines is $(\theta_a + \theta_b)$. As a result, the internal work absorbed at the yield lines is

$$M_p \cdot (2\theta_a + 2\theta_b)$$

“ M_p ” is the plastic capacity of the circular HSS wall bent about a yield line. From Figure... we observe the plastic moment capacity of the chord wall to be:

$$M_p = \left(\frac{t}{2} \cdot d \right) \cdot F_y \cdot \frac{t}{2} = \frac{t^2}{4} \cdot d \cdot F_y \quad (6-1)$$

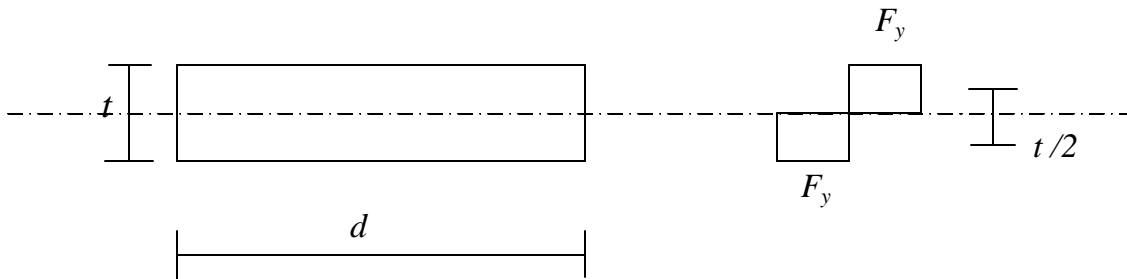


Figure 6.5 M_p Calculation Plot

As a condition for static equilibrium, the external and internal work is balanced, therefore

$$M_p \cdot (2\theta_a + 2\theta_b) = \frac{1}{2} w \cdot d \cdot \mathbf{d} \quad (6-2)$$

From geometry, the infinitesimal vertical displacement of the top point is

$$\mathbf{d} = a \cdot \mathbf{q}_a \cdot \sin \mathbf{a} + b \cdot \mathbf{q}_b \cdot \sin \mathbf{b} \quad (6-3)$$

And there is no horizontal displacement of the top point, so

$$a \mathbf{q}_a \cos \mathbf{a} - b \mathbf{q}_b \cos \mathbf{b} = 0 \quad (6-4)$$

Solving equations (6-2), (6-3) and (6-4) by canceling out \mathbf{q}_a , \mathbf{q}_b and \mathbf{d} , we can get:

$$wd = \frac{4M_p (a \cdot \cos \mathbf{a} + b \cdot \sin \mathbf{b})}{a \cdot b (\sin \mathbf{a} \cdot \sin \mathbf{b} + \cos \mathbf{a} \cdot \cos \mathbf{b})} = \frac{4M_p (a \cdot \cos \mathbf{a} + b \cdot \sin \mathbf{b})}{a \cdot b \cdot \cos(\mathbf{a} - \mathbf{b})} \quad (6-5)$$

Finally, a yield-line based closed form solution for calculating connection ultimate capacity through the use of the Upper Bound Theorem from the theory of plasticity is formulated from the nonlinear finite element modeling results. The form of the simplified design equation is:

$$wd = \frac{4M_p (a \cos \mathbf{a} + b \sin \mathbf{b})}{ab \cos(\mathbf{a} - \mathbf{b})} \quad (6-6)$$

Where,

$M_p \equiv$ the plastic capacity of the circular HSS wall bent about a hinge line causing plastification through the thickness of the wall;

$a \equiv$ the length of the line passing through the interior of the circular section and connecting the point at the tube mid-depth, at the unsaddled wall, and the point on the tube wall in contact with the extreme edge of the bearing saddle;

$b \equiv$ the length of the line passing through the interior of the circular section and connecting the point at the tube mid-depth, at the unsaddled wall, and the point on the tube wall directly under the line load;

\mathbf{a} \equiv the angle between the line with length of a and a vertical line;

\mathbf{b} \equiv the angle between the line with length of b and a horizontal line.

6.1.3 Bearing Capacity from the Estimation Equation

The results from the application of the estimation design equation (6-7) to the two geometries considered herein are presented as following.

6.1.3.1 Case -1

$$D = 660 \text{ mm}, t = 9.62 \text{ mm}, F_y = 344.75 \text{ N/mm}, d = 761.5 \text{ mm}$$

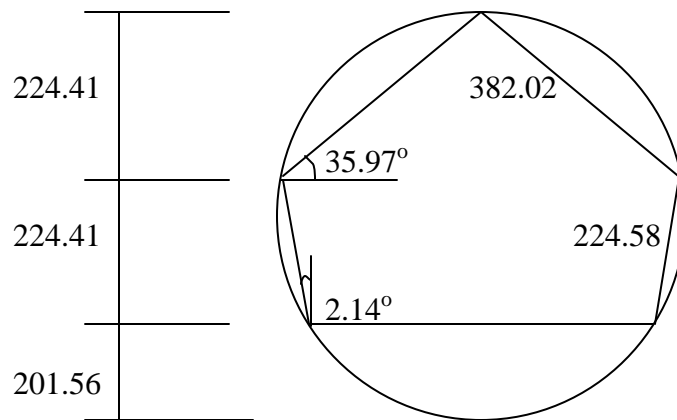


Figure 6.6 Schematic of HSS in Case -1

$$M_p = \frac{1}{4} \times 9.62^2 \times 761.5 \times 344.75 = 6.074 \times 10^6 \text{ N/mm}$$

$$a = 224.58 \text{ mm}, b = 382.02 \text{ mm}$$

$$\mathbf{a} = 2.14^\circ, \mathbf{b} = 35.97^\circ$$

$$wd = \frac{4M_p (a \cos \mathbf{a} + b \sin \mathbf{b})}{ab \cos(\mathbf{a} - \mathbf{b})} = 0.02519 M_p = 153004.1 \text{ N}$$

The analysis result from ABAQUS is: 168400N

The difference between the ABAQUS result and design equation result is:

$$\frac{168400 - 153004.1}{168400} = 9.1\%$$

6.1.3.2 Case -2

$$D = 660 \text{ mm}, t = 12.7 \text{ mm}, F_y = 344.75 \text{ N/mm}, d = 761.5 \text{ mm}$$

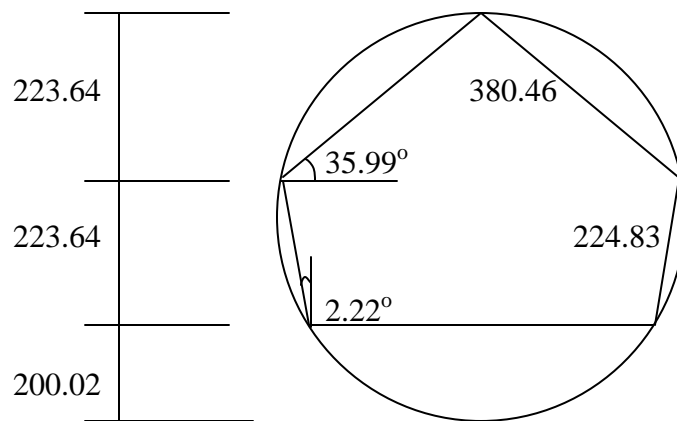


Figure 6.7 Schematic of HSS in Case -2

$$M_p = \frac{1}{4} \times 12.7^2 \times 761.5 \times 344.75 = 1.0586 \times 10^7 \text{ N/mm}$$

$$a = 223.83 \text{ mm}, b = 380.46 \text{ mm}$$

$$\mathbf{a} = 2.22^\circ, \mathbf{b} = 35.99^\circ$$

$$wd = \frac{4M_p (a \cos \mathbf{a} + b \sin \mathbf{b})}{ab \cos(\mathbf{a} - \mathbf{b})} = 0.02528M_p = 267614.1 \text{ N}$$

The analysis result from ABAQUS is: 304000N

The difference between the ABAQUS result and design equation result is:

$$\frac{304000 - 267614.1}{304000} = 11.97\%$$

It is very important and necessary for the estimation equation not only to be simple but also to agree with the ABAQUS analysis results. As can be seen from the results presented, the agreement between the crude energy balance method and the much more sophisticated nonlinear finite element approach is within 12 percent. It appears that this level of agreement may be sufficient for preliminary design calculations to be carried out using the simplified energy balance approach.

6.2 Connection Capacity from AISC

6.2.1 HSS-to-TEE Connection Capacity

In this section, all nominal capacities presented are consistent with the design strengths promulgated in the AISC Manual of Steel Construction (Third Edition) and AISC Hollow Structural Sections Connection Manual (1997).

The four limit states considered are:

- 1) flexural buckling of the TEE uprights as outlined in Section E2 of the Load and Resistance Factor Design Specification for Structural Steel Buildings;
- 2) flexural-torsional buckling of the TEE uprights as outlined in Section E3 of the Load and Resistance Factor Design Specification for Structural Steel Buildings;
- 3) cross-sectional shear failure of the HSS chord member as outlined in Section 5.2 of the Specification for the Design of Steel Hollow Structural Sections;
- 4) HSS wall transversely or longitudinally bearing failure as outlined in Section 8.1 and 8.2 of the Specification for the Design of Steel Hollow Structural Sections.

Table 6.1 Connection Cases Considered

Span	Pipe Diameter	Front Vertical
120-140	10x0.5	ST 4x11.5
120-140	12x0.5	ST 5x17.5
120-140	14x0.5	ST 5x17.5
140-160	14x0.5	ST 5x17.5
140-160	16x0.5	ST 6x25.0
140-160	20x0.5	ST 6x25.0
160-180	16x0.5	ST 6x25.0
160-180	20x0.5	ST 10x48.0
160-180	24x0.5	ST 10x48.0
80-200	24x0.562	ST 10x48.0
180-200	24x0.688	WT 10.5x73.5 & ST 10x48.0
180-200	24x0.938	WT 10.5x73.5

Table 6.2 TEE Properties

Front Vertical	Depth D	Stem Thickness tw	Flange		tf/tw	>1.1 ?	bf/D	>0.5 ?	check for FTB	bf/2/tf	λ_r for flanges	D/tw	λ_r for stems
			Width bf	Thickness tf									
ST 4x11.5	4.0	0.441	4.17	0.43	0.96	N	1.04	Y	Y	4.91 < 13.49	9.07 < 18.06		
ST 5x17.5	5.0	0.594	4.94	0.49	0.83	N	0.99	Y	Y	5.03 < 13.49	8.42 < 18.06		
ST 6x25.0	6.0	0.687	5.48	0.66	0.96	N	0.91	Y	Y	4.16 < 13.49	8.73 < 18.06		
ST 10x48.0	10.2	0.800	7.20	0.92	1.15	Y	0.71	Y	N	3.91 < 13.49	12.75 < 18.06		
WT 10.5x73.5	11.0	0.720	12.50	1.15	1.60	Y	1.14	Y	N	5.43 < 13.49	15.28 < 18.06		

All the TEE sections are compact.

Table 6.3 TEE Flexural Buckling Capacity

Span ft	HSS Chord in	Front Vertical	Ag in*in	kL in	rx in	ry in	λ_c	Fcr ksi	0.85*Fcr*Ag ksi
140	10 x 0.5	ST 4x11.5	3.38	63.04	1.22	0.795	1.05	31.57	90.70
140	12 x 0.5	ST 5x17.5	5.14	61.04	1.56	0.899	0.90	35.69	155.94
140	14 x 0.5	ST 5x17.5	5.14	59.04	1.56	0.899	0.87	36.48	159.37
160	14 x 0.5	ST 5x17.5	5.14	69.48	1.56	0.899	1.02	32.31	141.15
160	16 x 0.5	ST 6x25.0	7.32	67.48	1.85	1.030	0.87	36.53	227.30
160	20 x 0.5	ST 6x25.0	7.32	63.48	1.85	1.030	0.81	37.88	235.66
180	16 x 0.5	ST 6x25.0	7.32	77.91	1.85	1.030	1.00	32.91	204.75
180	20 x 0.5	ST 10x48.0	14.1	73.91	3.18	1.330	0.73	39.89	478.13
180	24 x 0.5	ST 10x48.0	14.1	69.91	3.18	1.330	0.69	40.85	489.64
200	24 x 0.562	ST 10x48.0	14.1	80.35	3.18	1.330	0.80	38.29	458.89
200	24 x 0.688	ST 10x48.0	14.1	80.35	3.18	1.330	0.80	38.29	458.89
200	24 x 0.688	WT 10.5x73.5	21.6	80.35	3.08	2.950	0.36	47.36	869.53
200	24 x 0.938	WT 10.5x73.5	21.6	80.35	3.08	2.950	0.36	47.36	869.53

Table 6.4 TEE Flexural-Torsional Buckling Capacity

Span ft	HSS Chord in	Front Vertical	Ag in ²	Fcry ksi	J in ⁴	r0 in	Fcrz ksi	H	Fcrft ksi	0.85*Ag*Fcrft ksi
140	10 x 0.5	ST 4x11.5	3.38	31.57	0.271	1.73	300.04	0.71	30.55	87.78
140	12 x 0.5	ST 5x17.5	5.14	35.69	0.633	2.23	277.36	0.65	34.04	148.72
140	14 x 0.5	ST 5x17.5	5.14	36.48	0.633	2.23	277.36	0.65	34.75	151.82
160	14 x 0.5	ST 5x17.5	5.14	32.31	0.633	2.23	277.36	0.65	30.96	135.26
160	16 x 0.5	ST 6x25.0	7.32	36.53	1.360	2.6	307.82	0.66	35.01	217.86
160	20 x 0.5	ST 6x25.0	7.32	37.88	1.360	2.6	307.82	0.66	36.24	225.49
180	16 x 0.5	ST 6x25.0	7.32	32.91	1.360	2.6	307.82	0.66	31.68	197.10
180	20 x 0.5	ST 10x48.0	14.1	39.89	4.160	4.36	173.83	0.63	36.30	435.06
180	24 x 0.5	ST 10x48.0	14.1	40.85	4.160	4.36	173.83	0.63	37.08	444.43
200	24 x 0.562	ST 10x48.0	14.1	38.29	4.160	4.36	173.83	0.63	34.98	419.29
200	24 x 0.688	ST 10x48.0	14.1	38.29	4.160	4.36	173.83	0.63	34.98	419.29
200	24 x 0.688	WT 10.5x73.5	21.6	47.36	7.690	4.63	186.01	0.85	45.13	828.65
200	24 x 0.938	WT 10.5x73.5	21.6	47.36	7.690	4.63	186.01	0.85	45.13	828.65

Table 6.5 HSS Shear Capacity

Span ft	HSS Chord in	Dia in	t in	Ag	λ D/t	λ_r 0.309E/Fy	a 225mm	a/D	Equation (5.2-1)	a/D<?	0.9*Vn
140	10 x 0.5	10	0.5	15.71	20.00	179.22	8.858	0.89	601.77	Y	212.06
140	12 x 0.5	12	0.5	18.85	24.00	179.22	8.858	0.74	381.49	Y	254.47
140	14 x 0.5	14	0.5	21.99	28.00	179.22	8.858	0.63	259.48	Y	296.88
160	14 x 0.5	14	0.5	21.99	28.00	179.22	8.858	0.63	259.48	Y	296.88
160	16 x 0.5	16	0.5	25.13	32.00	179.22	8.858	0.55	185.84	Y	339.29
160	20 x 0.5	20	0.5	31.42	40.00	179.22	8.858	0.44	106.38	Y	424.12
180	16 x 0.5	16	0.5	25.13	32.00	179.22	8.858	0.55	185.84	Y	339.29
180	20 x 0.5	20	0.5	31.42	40.00	179.22	8.858	0.44	106.38	Y	424.12
180	24 x 0.5	24	0.5	37.70	48.00	179.22	8.858	0.37	67.44	Y	508.94
200	24 x 0.562	24	0.562	42.37	42.70	179.22	8.858	0.37	90.33	Y	572.05
200	24 x 0.688	24	0.688	51.87	34.88	179.22	8.858	0.37	149.78	Y	700.30
200	24 x 0.688	24	0.688	51.87	34.88	179.22	8.858	0.37	149.78	Y	700.30
200	24 x 0.938	24	0.938	70.72	25.59	179.22	8.858	0.37	325.08	Y	954.77

Table 6.6 HSS Bearing Capacity

Span ft	HSS Chord in	Dia in	t in	Front Vertical	Longitudinal Length (in)	ϕR ksi	Transversal Length (in)	ϕR ksi	ϕR Min.
140	10 x 0.5	10	0.5	ST 4x11.5	4.0	68.75	4.17	94.38	68.75
140	12 x 0.5	12	0.5	ST 5x17.5	5.0	69.01	4.94	93.77	69.01
140	14 x 0.5	14	0.5	ST 5x17.5	5.0	68.08	4.94	87.51	68.08
160	14 x 0.5	14	0.5	ST 5x17.5	5.0	68.08	4.94	87.51	68.08
160	16 x 0.5	16	0.5	ST 6x25.0	6.0	68.36	5.48	86.50	68.36
160	20 x 0.5	20	0.5	ST 6x25.0	6.0	67.19	5.48	80.33	67.19
180	16 x 0.5	16	0.5	ST 6x25.0	6.0	68.36	5.48	86.50	68.36
180	20 x 0.5	20	0.5	ST 10x48.0	10.2	70.47	7.20	88.23	70.47
180	24 x 0.5	24	0.5	ST 10x48.0	10.2	69.14	7.20	82.56	69.14
200	24 x 0.562	24	0.562	ST 10x48.0	10.2	87.35	7.20	104.31	87.35
200	24 x 0.688	24	0.688	ST 10x48.0	10.2	130.91	7.20	156.32	130.91
200	24 x 0.688	24	0.688	WT 10.5x73.5	11.0	131.90	12.50	204.69	131.90
200	24 x 0.938	24	0.938	WT 10.5x73.5	11.0	245.16	12.50	380.47	245.16

Table 6.7 HSS-to-TEE Connection Capacity

Span ft	HSS Chord in	Front Vertical	Length Span/23-Dia in	Capacity of TEE		HSS Chord Shear Capacity ksi	HSS Chord Bearing Capacity ksi
				F.B. ksi	F.T.B. ksi		
140	10 x 0.5	ST 4x11.5	63.04	90.70	87.78	212.06	68.75
140	12 x 0.5	ST 5x17.5	61.04	155.94	148.72	254.47	69.01
140	14 x 0.5	ST 5x17.5	59.04	159.36	151.82	296.88	68.08
160	14 x 0.5	ST 5x17.5	69.48	141.15	135.26	296.88	68.08
160	16 x 0.5	ST 6x25.0	67.48	227.31	217.86	339.29	68.36
160	20 x 0.5	ST 6x25.0	63.48	235.66	225.49	424.12	67.19
180	16 x 0.5	ST 6x25.0	77.91	204.74	197.10	339.29	68.36
180	20 x 0.5	ST 10x48.0	73.91	478.12	435.06	424.12	70.47
180	24 x 0.5	ST 10x48.0	69.91	489.63	444.43	508.94	69.14
200	24 x 0.562	ST 10x48.0	80.35	458.90	419.28	572.05	87.35
200	24 x 0.688	ST 10x48.0	80.35	458.90	419.28	700.30	130.91
200	24 x 0.688	WT 10.5x73.5	80.35	869.53	828.65	700.30	131.90
200	24 x 0.938	WT 10.5x73.5	80.35	869.53	828.65	954.77	245.16

The last Table summarizes the capacities obtained for each of the member types considered in the analyses presented as antecedent tables on a member-by-member basis. It is observed the longitudinally bearing capacity of the circular HSS chord wall always governs the HSS-to-TEE connection capacity. Hence, the longitudinally bearing capacity of circular HSS is used to compare with the bearing capacity from ABAQUS and the yield-line theory based estimation equation. It is important to note that this limit state is currently not considered in the American Association of State Highway and Transportation Officials specification (2001).

6.2.2 Longitudinally Bearing Capacity from AISC

The longitudinally bearing capacities in the HSS sidewall of the two cases considered herein are presented below utilizing Equation (8.2.1) from the Specification for the Design of Steel Hollow Structural Sections, which appears as Equation 6-7.

$$\begin{aligned} \text{Design Strength } \phi R_n &= (1.0) \cdot \left\{ 5 F_y t^2 (1 + 0.25 N / D) Q_f \right\} & (6-7) \\ &= 5 \cdot 344.75 \cdot t^2 \cdot (1 + 0.25 \cdot 255 / 660) \\ &= 1890.25 \cdot t^2 \end{aligned}$$

Case-1: $t = 9.62 \text{ mm}$

$$\phi R_n = 1890.25 \cdot 9.62^2 = 174931.9N$$

Case-2: $t = 12.7 \text{ mm}$

$$\phi R_n = 1890.25 \cdot 12.7^2 = 304878.2N$$

6.3 Discussion of Results

The following discussion is solely related to the case of a WTEE bearing directly on a circular HSS chord member. As pointed out in the literature review, both the American (ASIC 1997) and Canadian (Packer and Henderson 1997) HSS specifications treat the cases of a transversely applied uniformly distributed line loading, oriented either parallel with, or perpendicular to, the circular HSS longitudinal axis. For the case of the WTEE bearing on a circular HSS member, the Canadian specification (Packer and Henderson 1997) points out that since the transverse capacity is so much greater than the longitudinal capacity, it is appropriate to base the connection capacity solely on the capacity computed with consideration of the longitudinal oriented component of the uniformly distributed line load (i.e. the portion imparted by the WTEE web, or stem, on the circular HSS wall).

The comparison of predicted WTEE bearing connection capacities from the AISC specification, yield-line based estimation equation, and nonlinear finite element model are presents in the Table 6.8.

Table 6.8 Comparison of Predicted WTEE Bearing Connection Capacities

Geometry <i>mm</i>	AISC (1997) <i>N</i>	Yield Line <i>N</i>	Finite Element Model <i>N</i>
D = 660, t = 9.62	174931.9	153004.1	168400
D = 660, t = 12.7	304878.2	267614.1	304000

For the case where D = 660 *mm* and t = 9.62 *mm*, the ratio of AISC predicted longitudinal bearing capacity to the ABAQUS WTEE bearing prediction is observed to be 1.04; whereas for

the case wherein $D = 660 \text{ mm}$ and $t = 12.7 \text{ mm}$, the ratio of AISC prediction to the ABAQUS prediction of nominal connection capacity is observed to be 1.00 (within two decimal places). However, with respect to the very simple and quick yield-line based energy approach obtained from the former work, the ratios of approximation prediction to nonlinear finite element analysis results are 0.91 and 0.88 for the respective cases mentioned earlier. As can be concluded from the results presented in this table, the approach promulgated by the Canadian HSS specification (Packer and Henderson 1997) and thus by default, the AISC 1997, to calculate the longitudinal bearing capacity indeed predict actual capacity (as reckoned by fully nonlinear finite element analysis).

While the agreement between the AISC and ABAQUS analysis results are closer to one another in their predicted ultimate capacities for the connection, it appears that the AISC predictions are consistently on the slightly un-conservative side. On the other hand, while the energy method yields a less favorable agreement that tends to be conservative in nature. Furthermore, while the AISC prediction is numerically close to the ABAQUS ultimate strength values, the failure mode assumed in the AISC approach differs significantly from the observed finite element model failure modes. As a result of this disagreement in the phenomenological features of the failure modes, it is surmised that the close agreement observed between the ABAQUS models and the AISC predictions are somewhat serendipitous in nature and might not be enjoyed across the entire permissible design space.

7.0 CONCLUSIONS AND RECOMMENDATIONS

Based on the analysis results obtained through the research related to the response of the connection region in tri-chord bridging at the points of attachment to the towers, the following conclusions and recommendations are made.

7.1 Validity of ABAQUS Modeling Techniques

Two out of ten experiment tests performed by Boone et al. on double-tee tubular joints were selected to serve as the standard against which to verify the robustness of the ABAQUS modeling techniques. In general, the finite element results agree with results from the tests very well. The finite element models tend to slightly under-predict the ultimate strength of the double-tee assemblies: the differences are less than 4.0%. Although the finite element models tend to predict a stiffer response in the elastic range than what was reported by Boone et al., the deviation is not so important since experiment procedure rather than an underlying shortcoming in finite element techniques may be the root cause for the overly stiff response. The validity of the finite element modeling techniques is supported from the validation study.

7.2 Yield-Line based Capacity Estimation Equation

A yield-line based closed form solution for calculating the bearing capacity of the circular hollow structural chord section loaded by an upright WTEE immediately adjacent to the column-chord connection in tri-chord sign structures is deduced utilizing the Upper Bound Theorem after observing the failure mode from ABAQUS modeling results.

The agreement between the crude estimation method and the much more sophisticated nonlinear finite element approach is within 12 percent. Given the simplicity in formulation and

execution of hand calculations, this approximate method provides reasonably good results that are suitable for design office calculations. Although bearing capacities predicted by this approximate equation are always smaller than results from ABAQUS analyses this is not seen as a drawback since conservatism is a desirable feature of approximate calculations.

Nevertheless, since this estimation equation indeed provides a less favorable agreement with ABAQUS modeling results, there are many subjects remained for future study. First of all, a more sophisticated collapse mechanism needs to be proposed to enhance the ability of yield-line theory to predict the bearing capacity. In addition, only bending energy terms were introduced to the overall energy balance equations to identify the ultimate load. Axial force energy terms and shear energy terms may also be considered in the energy balance equation.

7.3 Checking WTEE Bearing Capacity Using the AISC Specification

The existing AISC Specification provisions for the calculation of nominal capacity in a circular HSS member longitudinally loaded by a uniformly distributed line loading of finite length may successfully be applied to the case where connection capacity is required for a WTEE bearing directly against the wall of a circular HSS chord member at the connection region adjacent to the tower region of tri-chord sign structures. It is recommended that the overall depth of the constituent cross-sectional plate component of the WTEE member, which is oriented parallel to the longitudinal axis of the circular HSS member, be used as the length of the line load applied in the AISC predictive equation. While the AISC approach appears to be slightly un-conservative in terms of its predicted nominal connection capacity, it is still vastly superior to making no check at all; the situation currently perpetuated by the AASHTO Specification.

7.4 Flat Bearing Seat Connection Problem

Given that the flat bearing seat connection, instead of the fabricated saddle seat connection, has been widely used in sign structures throughout the Commonwealth prior to the failure in District 6 described in Chapter 1, it is important to evaluate the strength of this detail and provide a design equation useful to engineers working on predicting actual reserve strengths in such connections in the case of signage replacement / retro-fit, extreme event studies, etc.

Neither the American (AISC 1997) nor the Canadian (Packer and Henderson 1997) HSS specifications contain a predictive equation that is intended to provide the nominal capacity of a circular HSS member loaded transversely through a flat plate, which should be a subject of future study and research.

APPENDICES

APPENDIX A

Input File of WTEE Bearing Model

```
*HEADING
USE S4R SHELL ELEMENTS AND B33 BEAM ELEMENTS
89 ELEMENTS IN CIRCUMFERENCE; 160 ELEMENTS ALONG THE AXIS
TUBE: D=660, t=12.7
UNITS:N-MM
```

```
-----
**
**DEFINE NODES
**
*NODE,NSET=ENDN
1,0,-323.65,-225
801,0,-323.65,3300
320401,0,323.65,-225
321201,0,323.65,3300
640000,0.044365,-323.649997,-225
640800,0.044365,-323.649997,3300
650000,0,0,-225
650001,0,0,3300
*NGEN,NSET=CIRL1,LINE=C
1,320401,801,650000,,0,0,-1
*NGEN,NSET=CIRL2,LINE=C
320401,640000,801,650000,,0,0,-1
*NGEN,NSET=CIRR1,LINE=C
801,321201,801,650001,,0,0,-1
*NGEN,NSET=CIRR2,LINE=C
321201,640800,801,650001,,0,0,-1
*NFILL,NSET=CYLINDER
CIRL1,CIRR1,800,1
*NFILL,NSET=CYLINDER
CIRL2,CIRR2,800,1
*NSET,NSET=PIN,GENERATE
3225,118569,7209
3230,118574,7209
3235,118579,7209
```

3240,118584,7209
3245,118589,7209
3250,118594,7209
3255,118599,7209
3260,118604,7209
3265,118609,7209
3270,118614,7209
3275,118619,7209
3280,118624,7209
3285,118629,7209
522273,637617,7209
522278,637622,7209
522283,637627,7209
522288,637632,7209
522293,637637,7209
522298,637642,7209
522303,637647,7209
522308,637652,7209
522313,637657,7209
522318,637662,7209
522323,637667,7209
522328,637672,7209
522333,637677,7209

*NODE,NSET=BEAMN

650001,0,0,3300
650002,0,0,26200
650003,0,0,49100
650004,0,0,72000

*NODE

700001,-90.73,1323.65,524.06
700081,90.73,1323.65,524.06
716120,-90.73,328.65,524.06
716200,90.73,328.65,524.06

*NGEN,NSET=TF1

700001,700081,1

*NGEN,NSET=TF2

716120,716200,1

*NFILL,NSET=TFN

TF1,TF2,199,81

*NODE

716201,-90.73,323.65,524.06
716240,-2.286,323.65,524.06
716242,2.286,323.65,524.06
716281,90.73,323.65,524.06

```

*NGEN,NSET=TFN
716201,716240,1
*NGEN,NSET=TFN
716242,716281,1
*NODE,NSET=TFN
716282,-90.73,318.67,524.06
716283,90.73,318.67,524.06
716284,-90.73,313.51,524.06
716285,90.73,313.51,524.06
***
*NODE
800001,0,1323.65,281.72
800055,0,1323.65,519.65
811145,0,328.65,281.72
811199,0,328.65,519.65
*NGEN,NSET=TW1
800001,800055,1
*NGEN,NSET=TW2
811145,811199,1
*NFILL,NSET=TWN
TW1,TW2,199,56
***
*NODE
660001,0,1323.65,444.56
660002,0,2073.65,444.56
660003,0,2823.65,444.56
**
**DEFINE ELEMENTS##
**
*ELEMENT,TYPE=B33,ELSET=BEAME
650001,650001,650002
650002,650002,650003
650003,650003,650004
***
*ELEMENT,TYPE=S4R
1,3205,3210,10419,10414
14081,637597,637602,3210,3205
*ELGEN,ELSET=CYLINDER
1,160,5,1,88,7209,160
14081,160,5,1,1,0,0
***
***
*ELEMENT,TYPE=S4R
700001,700001,700406,700416,700011
*ELGEN,ELSET=TFE
700001,8,10,1,39,405,8

```

*ELEMENT,TYPE=S4R,ELSET=TFE
700313,715806,715796,291735,298944
700314,715816,715806,298944,306153
700315,715826,715816,306153,313362
700316,715836,715826,313362,320571
700317,715846,715836,320571,327780
700318,715856,715846,327780,334989
700319,715866,715856,334989,342198
700320,715876,715866,342198,349407

*ELEMENT,TYPE=S4R
800001,800281,800001,800006,800286
800040,320516,810921,810926,320521

*ELGEN,ELSET=TWE

800001,39,280,1,10,5,40

800040,10,5,40,1,0,0

*ELEMENT,TYPE=S4R,ELSET=TWE

800401,700041,700446,800331,800051
800402,700446,700851,800611,800331
800403,700851,701256,800891,800611
800404,701256,701661,801171,800891
800405,701661,702066,801451,801171
800406,702066,702471,801731,801451
800407,702471,702876,802011,801731
800408,702876,703281,802291,802011
800409,703281,703686,802571,802291
800410,703686,704091,802851,802571
800411,704091,704496,803131,802851
800412,704496,704901,803411,803131
800413,704901,705306,803691,803411
800414,705306,705711,803971,803691
800415,705711,706116,804251,803971
800416,706116,706521,804531,804251
800417,706521,706926,804811,804531
800418,706926,707331,805091,804811
800419,707331,707736,805371,805091
800420,707736,708141,805651,805371
800421,708141,708546,805931,805651
800422,708546,708951,806211,805931
800423,708951,709356,806491,806211
800424,709356,709761,806771,806491
800425,709761,710166,807051,806771
800426,710166,710571,807331,807051
800427,710571,710976,807611,807331
800428,710976,711381,807891,807611

```

800429,711381,711786,808171,807891
800430,711786,712191,808451,808171
800431,712191,712596,808731,808451
800432,712596,713001,809011,808731
800433,713001,713406,809291,809011
800434,713406,713811,809571,809291
800435,713811,714216,809851,809571
800436,714216,714621,810131,809851
800437,714621,715026,810411,810131
800438,715026,715431,810691,810411
800439,715431,715836,810971,810691
800440,715836,320571,320566,810971
*ELEMENT,TYPE=B33,ELSET=TBEAME
660001,660001,660002
660002,660002,660003
**
**DEFINE SECTION##
**
*SHELL SECTION,ELSET=CYLINDER,MATERIAL=STEEL
12.7,7
*SHELL SECTION,ELSET=TT,MATERIAL=STEEL
12.7,7
*SHELL SECTION,ELSET=TFE,MATERIAL=STEEL
23.368,7
*SHELL SECTION,ELSET=TWE,MATERIAL=STEEL
20.192,7
**
*BEAM SECTION,SECTION=PIPE,ELSET=BEAME,MATERIAL=STEEL
660.0,9.62
1.,0.,0.
*BEAM SECTION,SECTION=I,,ELSET=TBEAME,MATERIAL=STEEL
178.31,257.81,0.,182.88,0.,23.368,20.192
0.,0.,1.
***
***
*MATERIAL,NAME=STEEL
*ELASTIC
2.0E5,0.3
*PLASTIC
344.75,0.
354.024,0.00922948
517.125,0.0557238
551.6,0.090034
**
**MPC
**

```

*MPC

BEAM,801,650001
BEAM,16821,650001
BEAM,32841,650001
BEAM,48861,650001
BEAM,64881,650001
BEAM,80901,650001
BEAM,96921,650001
BEAM,112941,650001
BEAM,128961,650001
BEAM,144981,650001
BEAM,161001,650001
BEAM,177021,650001
BEAM,193041,650001
BEAM,209061,650001
BEAM,225081,650001
BEAM,241101,650001
BEAM,257121,650001
BEAM,273141,650001
BEAM,289161,650001
BEAM,305181,650001
BEAM,321201,650001
BEAM,337221,650001
BEAM,353241,650001
BEAM,369261,650001
BEAM,385281,650001
BEAM,401301,650001
BEAM,417321,650001
BEAM,433341,650001
BEAM,449361,650001
BEAM,465381,650001
BEAM,481401,650001
BEAM,497421,650001
BEAM,513441,650001
BEAM,529461,650001
BEAM,545481,650001
BEAM,561501,650001
BEAM,577521,650001
BEAM,593541,650001
BEAM,609561,650001
BEAM,625581,650001

*MPC

BEAM,800001,660001
BEAM,800006,660001
BEAM,800011,660001
BEAM,800016,660001

```
BEAM,800021,660001
BEAM,800026,660001
BEAM,800031,660001
BEAM,800036,660001
BEAM,800041,660001
BEAM,800046,660001
BEAM,800051,660001
BEAM,700001,660001
BEAM,700011,660001
BEAM,700021,660001
BEAM,700031,660001
BEAM,700041,660001
BEAM,700051,660001
BEAM,700061,660001
BEAM,700071,660001
BEAM,700081,660001
***
***
*BOUNDARY
PIN,PINNED
650004,1,3
650004,6
***
***
*STEP,NLGEOM,INC=20
*STATIC,RIKS
0.0001,1.
*CLOAD
660003,2,-4000000.0
*RESTART,WRITE,FREQUENCY=1
*ELPRINT,FREQUENCY=0
*NODE PRINT,FREQUENCY=0
*END STEP
```

APPENDIX B

.STA File of WTEE Bearing Model

Case-1: t = 9.62

SUMMARY OF JOB INFORMATION:

STEP	INC	ATT	SEVERE DISCON ITERS	EQUIL ITERS	TOTAL ITERS	TOTAL TIME/ FREQ	STEP TIME/LPF	INC OF TIME/LPF	DOF MONITOR	IF RIKS
1	1	1	0	3	3		0.000100	9.998e-005		R
1	2	1	0	3	3		0.000200	9.991e-005		R
1	3	1	0	3	3		0.000350	0.0001498		R
1	4	1	0	3	3		0.000574	0.0002245		R
1	5	1	0	3	3		0.000910	0.0003363		R
1	6	1	0	3	3		0.00141	0.0005034		R
1	7	1	0	3	3		0.00217	0.0007528		R
1	8	1	0	3	3		0.00329	0.001124		R
1	9	1	0	3	3		0.00497	0.001675		R
1	10	1	0	3	3		0.00745	0.002486		R
1	11	1	0	3	3		0.0111	0.003670		R
1	12	1	0	4	4		0.0164	0.005265		R
1	13	2	0	4	4		0.0191	0.002756		R
1	14	1	0	6	6		0.0229	0.003774		R
1	15	2	0	5	5		0.0236	0.0006591		R
1	16	1	0	5	5		0.0240	0.0004132		R
1	17	2	0	4	4		0.0240	4.454e-005		R
1	18	1	0	4	4		0.0241	3.141e-005		R
1	19	1	0	4	4		0.0241	2.717e-005		R
1	20	1	0	4	4		0.0241	-1.968e-005		R

Case-2: t =12.7

SUMMARY OF JOB INFORMATION:

STEP	INC	ATT	SEVERE DISCON ITERS	EQUIL ITERS	TOTAL ITERS	TOTAL TIME/ FREQ	STEP TIME/LPF	INC OF TIME/LPF	DOF MONITOR	IF RIKS
1	1	1	0	2	2		0.000100	0.0001000		R
1	2	1	0	2	2		0.000200	9.998e-005		R
1	3	1	0	2	2		0.000350	0.0001500		R
1	4	1	0	3	3		0.000575	0.0002249		R
1	5	1	0	3	3		0.000912	0.0003373		R
1	6	1	0	3	3		0.00142	0.0005058		R
1	7	1	0	3	3		0.00218	0.0007584		R
1	8	1	0	3	3		0.00331	0.001137		R
1	9	1	0	3	3		0.00502	0.001703		R
1	10	1	0	3	3		0.00757	0.002551		R
1	11	1	0	3	3		0.0114	0.003818		R
1	12	1	0	3	3		0.0171	0.005708		R
1	13	1	0	3	3		0.0256	0.008517		R
1	14	1	0	4	4		0.0382	0.01257		R
1	15	1	0	5	5		0.0555	0.01729		R
1	16	1	0	5	5		0.0682	0.01274		R
1	17	1	0	5	5		0.0743	0.006037		R
1	18	1	0	5	5		0.0760	0.001757		R
1	19	2	0	4	4		0.0760	-8.390e-006		R
1	20	1	0	4	4		0.0759	-0.0001396		R

BIBLIOGRAPHY

BIBLIOGRAPHY

1. AASHTO (2001) Standard Specifications for Structural Supports for Highway Signs, Luminaries and Traffic Signals, 4th Edition, American Association of State Highway and Transportation Officials, Inc., Washington D.C.
2. ABAQUS/STANDSARD Use's Manual 6.2 (2001), Hibbitt, Karlsson & Sorensen, Inc., Pawtucket, Rhode Island.
3. AISC (1997) Hollow Structural Sections Connections Manual, American Institute of Steel Construction, Chicago, Illinois.
4. AISC (Third Edition) Manual of Steel Construction, Load and Resistance Factor Design, American Institute of Steel Construction, Chicago, Illinois.
5. Boone, T.J., Yura, J.A., Hoadley, P.W. (1982) Chord Stress Effects on the Ultimate Strength of Tubular Joints, Phase I Report, Phil M. Ferguson Structural Engineering Laboratory, University of Texas at Austin, Austin, Texas.
6. Chakrabarty, J., (1987), Theory of Plasticity, McGraw-Hill Book Company, Incorporated, New York City, New York, p.229.
7. Coutie, M.G., Saidani, M. (1989) "The Use of Finite Element Techniques for the Analysis of RHS Structures with Flexible Joints," Proceedings of the 3rd International Symposium on Tubular Structures, Lappeenranta, Finland, pp. 224-231.
8. Coutie, M.G., Saidani, M. (1991) "Comparison of the Theoretical Behavior of Two Rectangular Hollow Section Trusses," Proceedings of the 4th International Symposium on Tubular Structures, Delft, The Netherlands, pp. 334-343.
9. Czechowski, A., Gasparski, T., Zycinski, J., Brodka, J. (1984) "Investigation into the Static Strength and Behavior of Latticed Girders Made of RHS," Document Number XV-E-052-84, International Institute of Welding, Paris, France.
10. Davies, G., Packer, J.A., (1982) "Predicting the Strength of Branch Plate – RHS Connections for Punching Shear," Canadian Journal of Civil Engineering, National Research Council of Canada, Vol. 9, Ottawa, Canada, pp. 458-467.

11. Frater, G.S., Packer, J.A., (1992) "Modeling of Hollow Structural Section Trusses," Canadian Journal of Civil Engineering, National Research Council of Canada, Vol. 19, Ottawa, Canada, pp. 947-959.
12. Gerard, G., (1962) Introduction to Structural Stability Theory, McGraw-Hill Book Company, Incorporated, New York City, New York.
13. Kapp, R.H., (1974) "Yield Line Analysis of a Web Connection in Direct Tension," Engineering Journal, American Institute of Steel Construction, Vol. 11, No. 2, Chicago, Illinois, pp.38-41.
14. Lau, B., (1987) "Statical Behavior of Square Chord Cropped Web Warren Truss Joints," Ph.D. Dissertation, Department of Civil Engineering, University of Manitoba, Winnipeg, Manitoba.
15. Packer, J.A., Davies, G., Coutie, M.G., (1980) "Yield Strength of Gapped Joints in Rectangular Hollow Section Trusses," Proceedings of the Institution of Civil Engineers, Part 2, Vol. 69, London, Great Britain, pp.995-1013.
16. Packer, J.A., Davies, G., Coutie, M.G., (1982) "Ultimate Strength of Gapped Joints in RHS Trusses," Journal of the Structural Division, American Society of Civil Engineers, Vol. 108, No. ST2, New York City, New York, pp.411-431.
17. Packer, J.A., Henderson, J.E. (1997) Hollow Structural Section Connections and Trusses, second edition, Design Guide, Canadian Institute of Steel Construction, Willowdale, Ontario, Canada.
18. PENNDOT (1996) "Overhead Sign Structures; 2 post and 4 post tri-chord truss spans from 18,000 to 72,000; Notes and Design Criteria, BD 644-M, Commonwealth of Pennsylvania Department of Transportation, Harrisburg, Pennsylvania.
19. Philiastides, A. (1988) "Fully Overlapped Rolled Hollow Section Welded Joints in Trusses," Ph.D. Dissertation, Department of Civil Engineering, University of Nottingham, Nottingham, United Kingdom.
20. Schilling, C.G., (1965) "Buckling Strength of Circular Tubes," Journal of the Structural Division, Proceedings of the American Society of Civil Engineers, Vol. 91, No. ST5, New York, New York, U.S.A.
21. Stockwell, F.W., (1974) "Yield Line Analysis of Column Webs with Welded Beam Connections," Engineering Journal, American Institute of Steel Construction, Vol. 11, No. 1, Chicago, Illinois, pp. 12-17.
22. Stockwell, F.W., (1975) "Discussion on: Yield Line Analysis of Column Webs with Welded Beam Connections," Engineering Journal, American Institute of Steel Construction, Vol. 12, No. 4, Chicago, Illinois, p.151.